Training Local Models from Reanalysis Data to Estimate Reference Evapotranspiration with Fewer Onsite Sensors, an Evaluation in West Africa

Jérémy Lavarenne, Audrey Brouillet

Title

Training local models from reanalysis data to estimate reference evapotranspiration with fewer onsite sensors, an evaluation in West Africa

Authorship

Jérémy LAVARENNE[1,2,*] (0000-0002-1954-4150), Audrey BROUILLET[3] (0000-0001-9466-0197)

[1] CIRAD, UMR TETIS, Montpellier, FR

[2] TETIS, Univ Montpellier, AgroParisTech, CIRAD, CNRS, INRAE, Montpellier, FR

[3] IRD, Espace Dev joint research unit, Maison de la Télédétection, 34000 Montpellier, FR

* corresponding author, jeremy.lavarenne@cirad.fr

Abstract

This study addresses the critical need for accurate reference evapotranspiration (ET0) estimation in data-scarce environments such as West Africa, where rapid population growth and climate change intensify water resource challenges. Traditionally, computing ET0 with the FAO-56 Penman-Monteith method requires multiple meteorological inputs—such as solar radiation, humidity, and wind speed—collected from costly, fully instrumented weather stations. However, the availability and maintenance of such equipment can be prohibitive in remote regions. To overcome these constraints, we explore the potential of machine learning (ML), specifically XGBoost (XGB) models, trained on NASA Power climate reanalysis datasets. Our approach relies on a limited subset of easily measured in situ variables—daily minimum and maximum temperatures and rainfall—to estimate ET0. Departing from standard ML practices that depend on short-term, site-specific data, we leverage the extensive historical

depth and broad spatial coverage of reanalysis products. We trained and validated twenty locally adapted XGB models using measurements from twenty diverse West African weather stations. Our results show that certain XGB model configurations, notably those incorporating temperature and rainfall data, can approximate ET0 estimates from the FAO-56 Penman-Monteith equation with median RMSE values frequently below 1 mm/day—levels comparable to commonly employed empirical formulas. This finding demonstrates that minimal on-site instrumentation, combined with ML and reanalysis data, can effectively support irrigation scheduling and enhance water-use efficiency under varying agro-ecological conditions. To foster broader implementation, we have released our XGB-ET0 code under the GPLv3 licence (https://github.com/SARRA-cropmodels/RF-ET0), enabling researchers and practitioners to locally train and deploy these models, thereby improving ET0 estimation and sustainable agricultural water management in resource-limited settings.

Keywords

- Evapotranspiration estimation
- Machine learning
- Precision irrigation
- XGBoost models
- Reanalysis datasets
- FAO-56 Penman-Monteith
- West Africa

1. Introduction

Accurately estimating actual evapotranspiration (ETa) is critical for optimizing irrigation practices and promoting sustainable agricultural water management. This need is particularly acute in West Africa, where growing population pressures and increasing variability in water

availability caused by climate change (Arnell and Lloyd-Hughes, 2014; Ayers et al., 2023; Brouillet and Sultan, 2023; Satgé et al., 2020) have intensified demands on limited water resources. Precision irrigation (PI), which tailors water inputs to compensate for ETa, offers a promising solution to reduce excessive irrigation, even in humid environments (Adeyemi et al., 2017; González Perea et al., 2018). Beyond irrigation scheduling, reliable ETa estimates play a pivotal role in understanding the water cycle, modeling water availability, and predicting changes in hydrological conditions. ETa is also a key input in process-based crop models, helping farmers anticipate the impact of different irrigation strategies on yields and overall water usage (Gu et al., 2020; Lopez-Jimenez et al., 2022; Pereira et al., 2020). Consequently, improving ETa estimation methods under data-scarce conditions is essential for both advancing scientific understanding and informing practical water management decisions in the region.

However, direct experimental methods for estimating ETa often require complex instrumentation, careful handling, and trained personnel, making them difficult to deploy and maintain (Li et al., 2009; Valayamkunnath et al., 2018). As a result, indirect ETa estimation methods have been developed, including several mathematical formulations based on meteorological variables (compiled in (McMahon et al., 2013)). Some of these methods rely on the concept of reference crop evapotranspiration (ET_0), which represents the amount of water lost to the atmosphere by a reference healthy, well-watered grass or alfalfa cover; this ET_0 is further modulated by a crop and growth stage-specific coefficient (crop coefficient, symbolised as Kc), to provide an estimate of actual evapotranspiration (noted ET_0). This ET_0, which represents the climate forcing component and is a widely used variable in crop water modelling and management, can be computed based on air temperature, solar radiation, relative humidity, and wind speed using the FAO-56 standardized Penman-Monteith equation (FAO-56-PM) (Richard G. Allen et al., 1998), the most widely-used procedure for estimating the ET_0 value.

However, obtaining all the meteorological variables required by the FAO-56-PM equation can be challenging. The cost, maintenance, and limited availability of fully

instrumented weather stations restrict the widespread calculation of ET_0, especially in developing countries (Djaman et al., 2016, 2015; Fisher and Pringle Iii, 2013; Valipour, 2015). To circumvent these constraints, a range of empirical ET_0 estimation models requiring fewer input variables has emerged (McMahon et al., 2013). While these simplified approaches can reduce the need for complex instrumentation, their accuracy varies markedly depending on local agroclimatic conditions (Djaman et al., 2015; Tabari and Talaee, 2011; Xystrakis and Matzarakis, 2011). Consequently, selecting and calibrating an appropriate empirical model for a given site remains a non-trivial, expert-dependent process that complicates routine ET_0 estimation and its integration into decision support services.

This study explores whether leveraging climate reanalysis datasets can help overcome these challenges. We hypothesize that machine learning (ML) models trained exclusively on local and extensive historical coverage of reanalysis data, and used to predict ET_0 from a limited set of weather variables (from only a few meteorological instruments) can achieve ET_0 estimation accuracy comparable to established empirical formulas. If confirmed, this approach could significantly simplify ET_0 estimation by reducing instrumentation requirements and expanding applicability in data-scarce contexts.

Recent ML advancements have shown promise for deriving agroclimatic indicators, including ET_0, from limited meteorological inputs. Such estimations have been performed using methods like support vector machines (SVM), random forests (RF), Gaussian process regression (GPR), and artificial neural networks (ANN) (Chia et al., 2020; Hebbalaguppae Krishnashetty et al., 2021). Yet, most existing ML-based ET_0 models rely on short-term, site-specific datasets, limiting their generalizability (see **Supplementary Table 1**). To our knowledge, no previous work has utilized global climate reanalysis products—datasets generated by assimilating historical weather station data into global circulation models—for training ET_0 estimation models. Such reanalysis datasets provide near-global coverage of past weather conditions at various resolutions (often down to 0.5 degrees), sub-daily time steps, and spanning multiple decades.

In this paper, we explicitly test the hypothesis that ML models, trained from reanalysis data using only a few simple on-site measurements (e.g., daily minimum and maximum temperatures and rainfall), can achieve ET_0 estimation accuracies on par with widely used empirical methods. By tapping into the historical depth and spatial consistency of the NASA Power reanalysis dataset, we aim to develop locally adapted models capable of capturing the long-term statistical relationships underlying ET_0-PM. Confirming this hypothesis would greatly simplify the ET_0 estimation process, providing a practical and precise tool for routine agricultural management and crop modelling in regions with sparse meteorological infrastructure.

Unlike previous approaches limited by geographically sparse or short-term training datasets, our method exploits the rich spatiotemporal coverage of reanalysis data to train and evaluate locally adapted ML models systematically. Furthermore, we examine the sensitivity of model performance to different subsets of input variables—a dimension rarely explored in the literature. To evaluate our methodology, we train local extreme gradient boosting (XGB) models (chosen for their robustness in regression tasks, e.g., as shown in hydrological studies such as (Niazkar et al., 2024)) using NASA Power data. We then compare the ET_0 estimates generated by these models—under various combinations of meteorological inputs—with ET_0 values derived from the FAO-56-PM approach using ground measurements from twenty weather stations spread across West Africa. We assess model performance both statistically and qualitatively and discuss the implications of our findings for local calibration. Finally, we present a Python software module called RF-ET_0, allowing researchers and practitioners to easily train and apply these XGB models anywhere in the world.

2. Materials and methods

2.1. General workflow

The workflow for training, evaluating, and testing XGB models to estimate reference evapotranspiration (ET0) involved several key steps. First, ground truth ET0 values (ET0-PM-GT) were computed using the FAO-56 Penman-Monteith equation and daily meteorological data collected from weather stations. These included air temperature (TMIN, TMAX), wind speed, rainfall, relative humidity (HR), and solar radiation (IRRAD).

To complement these observations, daily time series data for each site were retrieved from the NASA Power reanalysis dataset, spanning 1979–2020. Using the same FAO-56 Penman-Monteith equation, ET0 values (ET0-PM-RM) were computed from the reanalysis data to serve as the target for model training. The reanalysis dataset was split into a training subset (historical data up to one year before station observations) and a validation subset (the period immediately preceding the observations).

XGBoost (XGB) models were trained locally for each site using combinations of meteorological variables derived from reanalysis data as input features (e.g., TMIN, TMAX, WIND, IRRAD), forming distinct model classes. Each model class represented the variable configurations measurable by different types of weather stations. Model training used default hyperparameters with 1000 boosting rounds for robust regression.

Model performance was evaluated on the validation dataset by comparing predicted ET0 values against ET0-PM-RM, using root mean square error (RMSE) and the coefficient of determination (R^2) as metrics. Finally, the trained models were tested against ground truth ET0 values (ET0-PM-GT) derived from station observations. Performance was assessed across agro-ecological zones to analyze variability and identify the most reliable variable combinations for different climatic conditions.

2.2. In situ meteorological datasets

For this study, we used the data from the archive of the AfricaRice weather station network (https://dataverse.harvard.edu/dataverse/Weather), providing a representative set of meteorological observations for West Africa, as the data provided from their agrometeorological stations is openly available, homogeneous, and quality controlled. We selected sites for which original metadata (coordinates and elevation) were provided, and containing all the necessary variables to compute ET_0 using the FAO-56 standardized Penman-Monteith equation: air temperature, rainfall, wind speed, vapour pressure, and global radiation. A total of twenty sites were retained for the study, (**Figure 1, Table 1**). spanning from 17°N, 18°W to 4°N, 18°E covering seven distinct agro-ecological zones as classified by the FAO Global Agro-ecological Zones V4, simplified (FAO and IIASA, 2021). Of these, seventeen sites fall within the "lowland tropics", further categorised into nine "humid", five "sub-humid", and three "semi-arid" zones; the remaining sites are distributed among "desert/arid climate", "land with severe soil/terrain constraints", and "land with ample irrigated soils" (**Figure 2**), ensuring a representative sample of the agro-ecological variability within West Africa, albeit with some underrepresentation of arid zones.

The duration of these records varies depending on the station, and spans from March 19, 2012, to December 31, 2020. **Table 2** describes dataset durations and periods considered for the analysis on each station. To establish a ground truth for reference evapotranspiration (ET_0-PM-GT), we utilised the FAO-56 standardized Penman-Monteith equation, implemented through the reference_ET function in the Python Crop Simulation Environment (PCSE) package v.5.4.0 (de Wit, 2023).

2.3. Climate reanalysis datasets

To complement our in-situ data, we sourced daily weather data from the NASA Power API, which offers a comprehensive depiction of long-term meteorological conditions at a

regional scale. The data for our measurement sites was retrieved using the NASAPowerWeatherDataProvider function of PCSE v.5.4.0. NASA Power provides a detailed dataset including solar parameters from the GEWEX/SRB 3.0 and the CERES FlashFlux versions 2 and 3 models, as well as meteorological parameters from the GMAO MERRA-2 and GEOS 5.12.4 FP-IT models on a granular 0.5° x 0.5° latitude/longitude grid. such as the NASA Prediction of Worldwide Energy Resources (NASA Power) (Sparks, 2018; Zhang et al., 2008).

For our study, the dataset spanned from January 1st, 1984, to June 1st, 2022. It included a range of daily meteorological variables crucial for our analysis: minimal temperature (TMIN), maximal temperature (TMAX), average temperature (TEMP), rainfall (RAIN), average wind speed (WIND), average vapour pressure (VAP), and global radiation (IRRAD). We computed daily reference evapotranspiration values from reanalysis model (ET_0-PM-RM) from these reanalysis model variables. This computation was done using the reference_ET function from PCSE v.5.4.0, integrating station-specific elevation data from the AfricaRice dataset metadata, instead of the broader 0.5° x 0.5° elevation averages typically provided by NASA Power.

2.4. XGB model training and validation

In this study, XGBoost (XGB) models were trained and validated using daily weather data from NASA Power for each of the twenty sites. We chose to work only with this family of models as there are recognized as robust and adapted to a variety of tasks. Furthermore, we wanted to focus on the comparison in the performance of models of the same nature, but including an increasing number of predictor variables, rather than comparing different model formalisms. To evaluate the feasibility and performance of this approach, in this work we will train twenty local XGB models using data from NASA Power, as its API and companion tools allow for very efficient requests. For each site, a data partitioning was done to split the data into training and validation subsets. Specifically, the training dataset included NASA Power

records until a year prior to the first on-site observations, while the days leading up to these first observations formed the validation dataset. The in-situ observations themselves served as the test set. The periods used for each site are detailed in **Table 2**.

Our approach utilised eleven distinct combinations of daily variables from the NASA Power reanalysis model, forming the basis for 11 XGB model classes (**Table 3**). The target output for these models was the ET_0-PM-RM value. Model training was conducted using XGBoost v1.6.2 (Chen and Guestrin, 2016) within a Python v3.9.6 environment. To optimise performance, we increased the number of boost rounds to 1000 while keeping other hyperparameters at their default settings.

The performance of each XGB model was assessed through two key metrics: root mean squared error (RMSE) and coefficient of determination (R^2). This evaluation involved comparing the XGB-estimated ET_0 values with the ET_0-PM-RM values from the validation set, allowing for a robust analysis of model precision and accuracy over the 20 locations.

2.5. Comparison of the locally-trained neural network estimation models with other ET_0 estimation methods

In this study, we benchmarked the performance of our locally-trained XGB models for estimating ET_0 against traditional empirical methods described in **Table 4**. This comparison was based on ET_0 calculations on test sets from in situ datasets (**Table 2)**. We employed two primary performance metrics for this analysis: the correlation coefficient and root mean square error (RMSE). These metrics were applied to evaluate both our neural network approach and the selected empirical formulas, with a focus on their accuracy in estimating ET_0-PM-GT across the twenty study sites.

To facilitate a comprehensive understanding of the results, we visualised the performance comparisons using Taylor diagrams. This graphical representation allowed us to simultaneously assess the correlation, standard deviation, and RMSE of the different methods.

Additionally, we conducted a qualitative analysis to provide deeper insights into the strengths and limitations of each approach in various agro-climatic conditions.

3. Results

3.1. Training and validation of the XGB models

In our study, an average of 10,000 records from NASA Power were utilised for each site to train the different XGB model classes presented in **Table 3**. Analysing the performance metrics against the validation sets (left-out training data from NASA Power), as detailed in **Table 5**, revealed distinct patterns in model efficacy. Notably, model class M11 emerged as the top performer, achieving a mean R^2 of 0.99 and a mean RMSE of just 0.09 mm. This superior performance aligns with our expectations, considering that M11's set of training variables - or features - closely mimics the variables used by the FAO56-PM- ET_0 formula. This suggests a high capability of XGB models to approximate the FAO56-PM- ET_0 method accurately.

Model classes M9 and M10 also demonstrated strong results, with R^2 values around 0.95, but their RMSEs were higher, approximately 0.15 mm. Model class M7, while showing promising results with a mean R^2 of 0.87, exhibited variability across different sites. In contrast, the least effective models (M1-M4) recorded R^2 values around 0.62 and an RMSE of 0.68 mm, indicating a lower level of performance.

These findings imply that the performance of ET_0-PM-RM estimation might vary with agro-ecological zones (AEZs) as the main driving factors of evapotranspiration are not identical in all environments. A notable observation was the underperformance of model class M7 in north-western sites, suggesting that adding more features could potentially enhance accuracy. Specifically, including the irradiance (IRRAD) feature in the models significantly improved ET_0 estimations by incorporating the radiative component, as evidenced by the improved validation metrics.

3.2. Comparison of the trained XGB performance against empirical ET_0 estimation formulas from ground data

Then, from the in-situ values of the test set, we calculated ET_0 using established empirical formulas (presented in **Table 4**), estimated ET_0 using our different XGB model classes, and compared these calculations with the ET_0 value computed using in situ weather measurements (ET_0-PM-GT) across the twenty sites (**Table 6**). The performance of each method was quantified using the root mean square error (RMSE) and correlation coefficient, with the results further illustrated in Taylor diagrams (representing correlation coefficient, RMSE and reference value in one plot) for a visual comparison (**Figure S1**).

A qualitative analysis was performed from these Taylor diagrams, in which we consider as a suitable model a model in which the RMSE was below 1 mm, and that is inside the highest available and the least high available correlation coefficient quadrant. The models were then scored and ranked based on their adherence to these criteria at each site (**Table 7**). According to the data, XGB model class 11 was distinguished as the most accurate, followed by the Irmak-a model. Subsequent ranks were shared by Hargreaves, Irmak-c, Valiantzas-a, and XGB-M8 models, which displayed comparable performance.

Notably, the Irmak-a model showed significant variability in RMSE across the sites, with a mean variability of 0.75, as opposed to 0.71 for M8 and 0.48 for M9. This variability is crucial as it affects the reliability and consistency of the model's performance in diverse climatic contexts, as represented by the various sites in West Africa.

4. Discussion

Our study contributes to the active research on machine learning (ML) methodologies for estimating ET_0 from a limited dataset of meteorological variables. In a field inclined towards the application of various ML approaches, we've selected XGB, and specifically extreme

gradient boosting (XGBoost) due to its proven robustness and established track record (Nielsen, 2016). Central to our discourse is the challenge of training data acquisition—a facet that, in our view, has not received due attention. The prevalent practice in the literature utilises weather data from a small number of locations over short time series to train models (see **Supplementary Table 1** for a curated selection of studies on the topic). These models are then expected to extrapolate ET_0 estimations to larger, often regional scales, which risks significant extrapolation errors during application.

We propose a methodological pivot, employing a transversal ML approach that utilises local meteorological data from assimilation databases. This strategy has the distinct advantage of being deployable in areas devoid of ground weather data, offering uniform datasets that boast extensive historical records and spatial representativity—crucial for models that need to operate across varied geographic expanses. We harnessed the breadth of NASA Power's data, spanning a grid resolution of 0.5° x 0.5°, effectively training a model for every ~3000km² under West Africa's latitudes. However, we acknowledge that such a resolution may not fully encapsulate the microclimatic diversity within these regions, especially in areas with complex terrain. One solution to this limitation could involve debiasing reanalysis data using historical ground measurements, potentially through methods such as linear regression, prior to training the ML models (Chandler, William S., 2011).

Moreover, our approach stands to be further refined by incorporating data from sources with finer resolutions, such as the fifth generation of European ReAnalysis climate products (Copernicus ERA5) (Hersbach et al., 2020; Muñoz-Sabater et al., 2021). This would offer a more detailed 0.1° x 0.1° resolution and an extensive historical reach back to 1950—allowing the inclusion of rarer climatic events in our training set, however at a price of lengthier API calls thus overall computation time. Such granularity is anticipated to enhance the representativeness of training data and, consequently, the performance of ML models, although this hypothesis warrants additional research to quantify the influence of training data volume on model performance.

For example, the Hargreaves-Samani model (George H. Hargreaves and Zohrab A. Samani, 1985), the Schendel model (Schendel, U., 1967), and the Priestley-Taylor model (Priestley and Taylor, 1972) are based only on solar radiation and air temperature values ; the Turc radiation-based model (Turc, L, 1961) uses temperature and relative humidity ; the Makkink-based models (Allen, Richard, 2003; Hansen, 1984; Makkink, G.F., 1957) use radiation-related parameters. A thorough review of these methods can be found in (McMahon et al., 2013).

Aiming to serve practitioners with scant meteorological infrastructure, our study sought to validate the accuracy and precision of XGB-based ET_0 estimation models against the FAO-56 standardized PM equation. Our experiments scrutinised the impact of a limited set of input variables on ET_0 output quality. We also compared the ML-derived ET_0 estimates with those calculated from ground truth data across diverse West African climates, ensuring our models' efficacy relative to conventional methods.

The practicality of our approach is underscored by its minimal data requirements: a farm manager equipped with only a min/max thermometer and a rain funnel shall be able to use a locally trained model to estimate ET_0 with a level of precision and accuracy usually attainable by also having anemometer or hygrometer readings. Existing literature suggests different combinations of variables for efficient ET_0 estimation by models : (Granata, 2019) suggests mean temperature, mean relative humidity, and net solar radiation; wind and sunny hours as the strict minimum information for most locations according to (Shabani et al., 2020), and most empirical formulas need at least information about wind speed plus deficit pressure or solar radiation with air temperature. Meanwhile, our approach showed that it can yield models that perform relatively well, starting with only information about minimum, maximum, and average daily air temperature. With a dependency on a high number of devices to measure each variable needed, there is a greater risk in data gaps leading to impossibility to calculate ET_0; this issue of missing or incomplete meteorological data has been discussed in (Koudahe et al., 2018). Our finding suggests that practitioners may only need a quality

thermometer for reliable ET_0 estimation, simplifying an on-farm weather data acquisition process that is already challenging in the region (Dinku, 2019). Stacking up variables will make the estimations more reliable. Compared to other models that overestimate ET_0, our models demonstrated better stability and less bias across various climates, although this observation necessitates further validation with a broader dataset. The use of twenty weather stations provides a solid foundation for our performance analysis, but a more expansive dataset would enable a more comprehensive understanding of the models' applicability and robustness.

Most of these empiric models have been initially defined in a given climatic environment and are less reliable or at least need recalibration when used in different climates. In the context of climate change, with anticipated shifts in climatic zones (Cui et al., 2021), our universally applicable method, supported by global assimilation data, could significantly aid in ET_0 estimation efforts. Our XGB- ET_0 models, though in need of further validation, show potential for at least equivalent performance compared to traditional empirical models, with the added benefit of being more robust across different AEZs. This robustness is particularly important in reducing bias risks, a common issue with empirical formulas lacking quality assessment avenues.

To enable wider application and continued research, we have made our XGB- ET_0 code publicly available under the GPLv3 licence (doi: 10.5281/zenodo.10463369, repository URL: https://github.com/SARRA-cropmodels/RF-ET0). This initiative allows researchers and practitioners to conduct their own localised model training and ET_0 estimations, utilising the model classes we've explored in this work.

Conclusion

This research represents a significant stride in the application of machine learning for agricultural water management, particularly within the challenging context of West Africa. The study has successfully demonstrated the efficacy of XGB models in estimating evapotranspiration (ET) using limited meteorological data. Our approach, which utilizes

extensive historical and spatial data from NASA Power's climate reanalysis datasets, marks a departure from traditional methods reliant on short-term, location-specific weather data. The ability of these models to accurately approximate ET estimations, as validated against ground measurements from diverse West African agro-ecological zones, underscores their potential in areas with limited meteorological infrastructure. This methodology not only simplifies the data requirements for ET estimation but also proves to be robust across various climatic conditions, enhancing its applicability for sustainable water management practices. The outcomes of this research contribute to the broader body of knowledge by showcasing the practicality of machine learning in agricultural contexts and underscore the importance of adopting innovative technologies in the face of climate change and resource constraints. The findings of this study hold significant implications for precision irrigation and water resource management, providing a sustainable and accessible solution to a region facing acute water-related challenges.

Data Statement

All data, models, or code generated or used during the study are available in a repository or online in accordance with funder data retention policies. Data used for validation is available at the DOIs indicated in **Table 2**. Additionally, the climate reanalysis datasets utilized in this study, provided by NASA Power, are publicly accessible and can be retrieved for extended time series and various spatial resolutions through their API and data services. The XGB- ET_0 code developed for this study is publicly available under the GPLv3 licence, ensuring open access and facilitating further research and practical applications. The code can be accessed at the following repository URL: https://github.com/SARRA-cropmodels/RF-ET0 (doi:10.5281/zenodo.10463369).

Acknowledgements

The meteorological data were obtained from the NASA Langley Research Center POWER Project funded through the NASA Earth Science Directorate Applied Science Program. The authors would like to thank Vincent SIMONNEAUX and Michel LE PAGE (CESBIO, Toulouse) and Gilles BELAUD (UMR G-EAU, Montpellier) for their contribution to the early versions of this manuscript. Also, they would like to thank Dino IENCO and Roberto INTERDONATO (UMR TETIS, Montpellier) for their feedback about the ML methodology.

Author contributions

- Jérémy LAVARENNE: Conceptualization, Methodology, Software, Formal Analysis, Investigation, Writing - Original draft, Visualization, Supervision
- Audrey BROUILLET: Conceptualization, Methodology, Writing - Review and editing

Funding

This research did not receive any specific grant from funding agencies in the public, commercial, or not-for-profit sectors.

References

Abtew, W., 1996. EVAPOTRANSPIRATION MEASUREMENTS AND MODELING FOR THREE WETLAND SYSTEMS IN SOUTH FLORIDA [1]. JAWRA J. Am. Water Resour. Assoc. 32, 465–473. https://doi.org/10.1111/j.1752-1688.1996.tb04044.x

Adeyemi, O., Grove, I., Peets, S., Norton, T., 2017. Advanced Monitoring and Management Systems for Improving Sustainability in Precision Irrigation. Sustainability 9, 353. https://doi.org/10.3390/su9030353

Allen, Richard, 2003. Crop Coefficients. Encycl. Water Sci. https://doi.org/10.1081/E-EWS 120010037

Arnell, N.W., Lloyd-Hughes, B., 2014. The global-scale impacts of climate change on water resources and flooding under new climate and socio-economic scenarios. Clim. Change 122, 127–140. https://doi.org/10.1007/s10584-013-0948-4

Ayers, J.R., Villarini, G., Tramblay, Y., Kim, H., 2023. Observed changes in monthly baseflow across Africa. Hydrol. Sci. J. 68, 108–118. https://doi.org/10.1080/02626667.2022.2144320

Brouillet, A., Sultan, B., 2023. Livestock exposure to future cumulated climate-related stressors in West Africa. Sci. Rep. 13, 2698. https://doi.org/10.1038/s41598-022-22544-y

Chandler, William S., 2011. Downscaling NASA Climatological Data to Produce Detailed Climate Zone Maps.

Chen, T., Guestrin, C., 2016. XGBoost: A Scalable Tree Boosting System, in: Proceedings of the 22nd ACM SIGKDD International Conference on Knowledge Discovery and Data Mining. pp. 785–794. https://doi.org/10.1145/2939672.2939785

Chia, M.Y., Huang, Y.F., Koo, C.H., Fung, K.F., 2020. Recent Advances in Evapotranspiration Estimation Using Artificial Intelligence Approaches with a Focus on Hybridization Techniques—A Review. Agronomy 10, 101. https://doi.org/10.3390/agronomy10010101

Cui, D., Liang, S., Wang, D., Liu, Z., 2021. A 1-km global dataset of historical (1979–2017) and future (2020–2100) Köppen-Geiger climate classification and bioclimatic variables (preprint). Data, Algorithms, and Models. https://doi.org/10.5194/essd-2021-53

Dalton, J, 1802. Experimental Essays on the Constitution of Mixed Gases: On the Force of Steam or Vapour from Water or Other Liquids in Different Temperatures, Both in a Torricelli Vacuum and in Air; on Evaporation; and on Expansion of Gases by Heat. Mem. Lit. Philos. Soc. Manch. 5, 536–602.

de Wit, 2023. PCSE: the Python crop simulation environment.

Dinku, T., 2019. Challenges with availability and quality of climate data in Africa, in: Extreme Hydrology and Climate Variability. Elsevier, pp. 71–80. https://doi.org/10.1016/B978-0-12-815998-9.00007-5

Djaman, K., Balde, A.B., Sow, A., Muller, B., Irmak, S., N'Diaye, M.K., Manneh, B., Moukoumbi, Y.D., Futakuchi, K., Saito, K., 2015. Evaluation of sixteen reference evapotranspiration methods under sahelian conditions in the Senegal River Valley. J. Hydrol. Reg. Stud. 3, 139–159. https://doi.org/10.1016/j.ejrh.2015.02.002

Djaman, K., Irmak, S., Kabenge, I., Futakuchi, K., 2016. Evaluation of FAO-56 Penman-Monteith Model with Limited Data and the Valiantzas Models for Estimating Grass-Reference Evapotranspiration in Sahelian Conditions. J. Irrig. Drain. Eng. 142, 04016044. https://doi.org/10.1061/(ASCE)IR.1943-4774.0001070

FAO, IIASA, 2021. Global Agro Ecological Zones version 4 (GAEZ v4).

Fisher, D.K., Pringle Iii, H.C., 2013. Evaluation of alternative methods for estimating reference evapotranspiration. Agric. Sci. 04, 51–60. https://doi.org/10.4236/as.2013.48A008

George H. Hargreaves, Zohrab A. Samani, 1985. Reference Crop Evapotranspiration from Temperature. Appl. Eng. Agric. 1, 96–99. https://doi.org/10.13031/2013.26773

González Perea, R., Daccache, A., Rodríguez Díaz, J.A., Camacho Poyato, E., Knox, J.W., 2018. Modelling impacts of precision irrigation on crop yield and in-field water management. Precis. Agric. 19, 497–512. https://doi.org/10.1007/s11119-017-9535-4

Granata, F., 2019. Evapotranspiration evaluation models based on machine learning algorithms—A comparative study. Agric. Water Manag. 217, 303–315. https://doi.org/10.1016/j.agwat.2019.03.015

Gu, Z., Qi, Z., Burghate, R., Yuan, S., Jiao, X., Xu, J., 2020. Irrigation Scheduling Approaches and Applications: A Review. J. Irrig. Drain. Eng. 146, 04020007. https://doi.org/10.1061/(ASCE)IR.1943-4774.0001464

Hansen, S., 1984. Estimation of Potential and Actual Evapotranspiration. Hydrol. Res. 15, 205–212. https://doi.org/10.2166/nh.1984.0017

Hebbalaguppae Krishnashetty, P., Balasangameshwara, J., Sreeman, S., Desai, S., Bengaluru Kantharaju, A., 2021. Cognitive computing models for estimation of reference evapotranspiration: A review. Cogn. Syst. Res. 70, 109–116. https://doi.org/10.1016/j.cogsys.2021.07.012

Hersbach, H., Bell, B., Berrisford, P., Hirahara, S., Horányi, A., Muñoz-Sabater, J., Nicolas, J., Peubey, C., Radu, R., Schepers, D., Simmons, A., Soci, C., Abdalla, S., Abellan, X., Balsamo, G., Bechtold, P., Biavati, G., Bidlot, J., Bonavita, M., De Chiara, G., Dahlgren, P., Dee, D., Diamantakis, M., Dragani, R., Flemming, J., Forbes, R., Fuentes, M., Geer, A., Haimberger, L., Healy, S., Hogan, R.J., Hólm, E., Janisková, M., Keeley, S., Laloyaux, P., Lopez, P., Lupu, C., Radnoti, G., De Rosnay, P., Rozum, I., Vamborg, F., Villaume, S., Thépaut, J., 2020. The ERA5 global reanalysis. Q. J. R. Meteorol. Soc. 146, 1999–2049. https://doi.org/10.1002/qj.3803

Irmak, S., Allen, R.G., Whitty, E.B., 2003a. Daily Grass and Alfalfa-Reference Evapotranspiration Estimates and Alfalfa-to-Grass Evapotranspiration Ratios in Florida. J. Irrig. Drain. Eng. 129, 360–370. https://doi.org/10.1061/(ASCE)0733-9437(2003)129:5(360)

Irmak, S., Irmak, A., Allen, R.G., Jones, J.W., 2003b. Solar and Net Radiation-Based Equations to Estimate Reference Evapotranspiration in Humid Climates. J. Irrig. Drain. Eng. 129, 336–347. https://doi.org/10.1061/(ASCE)0733-9437(2003)129:5(336)

Jensen, M.E., Haise, H.R., 1963. Estimating Evapotranspiration from Solar Radiation. J. Irrig. Drain. Div. 89, 15–41. https://doi.org/10.1061/JRCEA4.0000287

Koudahe, K., Djaman, K., Adewumi, J.K., 2018. Evaluation of the Penman–Monteith reference evapotranspiration under limited data and its sensitivity to key climatic variables under humid and semiarid conditions. Model. Earth Syst. Environ. 4, 1239–1257. https://doi.org/10.1007/s40808-018-0497-y

Li, Z.-L., Tang, R., Wan, Z., Bi, Y., Zhou, C., Tang, B., Yan, G., Zhang, X., 2009. A Review of Current Methodologies for Regional Evapotranspiration Estimation from Remotely Sensed Data. Sensors 9, 3801–3853. https://doi.org/10.3390/s90503801

Lopez-Jimenez, J., Vande Wouwer, A., Quijano, N., 2022. Dynamic Modeling of Crop–Soil Systems to Design Monitoring and Automatic Irrigation Processes: A Review with Worked Examples. Water 14, 889. https://doi.org/10.3390/w14060889

Mahringer, W., 1970. Verdunstungsstudien am Neusiedler See. Arch. Für Meteorol. Geophys. Bioklimatol. Ser. B 18, 1–20. https://doi.org/10.1007/BF02245865

Makkink, G.F., 1957. Testing the Penman formula by means of lysimeters. J. Inst. Water Eng. 11, 277–88.

McMahon, T.A., Peel, M.C., Lowe, L., Srikanthan, R., McVicar, T.R., 2013. Estimating actual, potential, reference crop and pan evaporation using standard meteorological data: a pragmatic synthesis. Hydrol. Earth Syst. Sci. 17, 1331–1363. https://doi.org/10.5194/hess-17-1331-2013

Muñoz-Sabater, J., Dutra, E., Agustí-Panareda, A., Albergel, C., Arduini, G., Balsamo, G., Boussetta, S., Choulga, M., Harrigan, S., Hersbach, H., Martens, B., Miralles, D.G., Piles, M., Rodríguez-Fernández, N.J., Zsoter, E., Buontempo, C., Thépaut, J.-N., 2021. ERA5-Land: a state-of-the-art global reanalysis dataset for land applications. Earth Syst. Sci. Data 13, 4349–4383. https://doi.org/10.5194/essd-13-4349-2021

Niazkar, M., Menapace, A., Brentan, B., Piraei, R., Jimenez, D., Dhawan, P., Righetti, M., 2024. Applications of XGBoost in water resources engineering: A systematic literature

499 review (Dec 2018–May 2023). Environ. Model. Softw. 174, 105971.
500 https://doi.org/10.1016/j.envsoft.2024.105971
501 Nielsen, D., 2016. Tree Boosting With XGBoost - Why Does XGBoost Win “Every” Machine
502 Learning Competition? Norwegian University of Science and Technology.
503 Oudin, Ludovic, 2004. Recherche d’un modèle d’évapotranspiration potentielle pertinent
504 comme entrée d’un modèle pluie-débit global. ENGREF (AgroParisTech).
505 Penman, H. L., 1963. Vegetation and Hydrology. Soil Sci. 96, 357.
506 Pereira, L.S., Paredes, P., Jovanovic, N., 2020. Soil water balance models for determining
507 crop water and irrigation requirements and irrigation scheduling focusing on the FAO56
508 method and the dual Kc approach. Agric. Water Manag. 241, 106357.
509 https://doi.org/10.1016/j.agwat.2020.106357
510 Priestley, C.H.B., Taylor, R.J., 1972. On the Assessment of Surface Heat Flux and
511 Evaporation Using Large-Scale Parameters. Mon. Weather Rev. 100, 81–92.
512 https://doi.org/10.1175/1520-0493(1972)100<0081:OTAOSH>2.3.CO;2
513 Richard G. Allen, Luis S. Pereira, Dirk Raes, Martin Smith, 1998. FAO Irrigation and drainage
514 paper No. 56. Rome Food Agric. Organ. U. N. 56, 26–40.
515 Rohwer, Carl, 1931. Evaporation from Free Water Surfaces. US Dep. Agric.
516 Satgé, F., Defrance, D., Sultan, B., Bonnet, M.-P., Seyler, F., Rouché, N., Pierron, F., Paturel,
517 J.-E., 2020. Evaluation of 23 gridded precipitation datasets across West Africa. J.
518 Hydrol. 581, 124412. https://doi.org/10.1016/j.jhydrol.2019.124412
519 Schendel, U., 1967. Vegetations wasserverbrauch und-wasserbedarf. Habilit. Kiel 1–11.
520 Shabani, S., Samadianfard, S., Sattari, M.T., Mosavi, A., Shamshirband, S., Kmet, T.,
521 Várkonyi-Kóczy, A.R., 2020. Modeling Pan Evaporation Using Gaussian Process
522 Regression K-Nearest Neighbors Random Forest and Support Vector Machines;
523 Comparative Analysis. Atmosphere 11, 66. https://doi.org/10.3390/atmos11010066
524 Sparks, A., 2018. nasapower: A NASA POWER Global Meteorology, Surface Solar Energy
525 and Climatology Data Client for R. J. Open Source Softw. 3, 1035.
526 https://doi.org/10.21105/joss.01035

Tabari, H., Talaee, P.H., 2011. Local Calibration of the Hargreaves and Priestley-Taylor Equations for Estimating Reference Evapotranspiration in Arid and Cold Climates of Iran Based on the Penman-Monteith Model. J. Hydrol. Eng. 16, 837–845. https://doi.org/10.1061/(ASCE)HE.1943-5584.0000366

Trabert, W, 1896. Neue beobachtungen über verdampfungsgeschwindigkeiten. Meteorol Z 13, 261–63.

Turc, L, 1961. Water requirements assessment of irrigation, potential evapotranspiration: Simplified and updated climatic formula. Ann. Agron. 12, 13–49.

Valayamkunnath, P., Sridhar, V., Zhao, W., Allen, R.G., 2018. Intercomparison of surface energy fluxes, soil moisture, and evapotranspiration from eddy covariance, large-aperture scintillometer, and modeling across three ecosystems in a semiarid climate. Agric. For. Meteorol. 248, 22–47. https://doi.org/10.1016/j.agrformet.2017.08.025

Valiantzas, J.D., 2013. Simple ET0 Forms of Penman's Equation without Wind and/or Humidity Data. II: Comparisons with Reduced Set-FAO and Other Methodologies. J. Irrig. Drain. Eng. 139, 9–19. https://doi.org/10.1061/(ASCE)IR.1943-4774.0000502

Valipour, M., 2015. Temperature analysis of reference evapotranspiration models: Reference evapotranspiration models. Meteorol. Appl. 22, 385–394. https://doi.org/10.1002/met.1465

Xystrakis, F., Matzarakis, A., 2011. Evaluation of 13 Empirical Reference Potential Evapotranspiration Equations on the Island of Crete in Southern Greece. J. Irrig. Drain. Eng. 137, 211–222. https://doi.org/10.1061/(ASCE)IR.1943-4774.0000283

Zhang, T., Chandler, W.S., Hoell, J.M., Westberg, D., Whitlock, C.H., Stackhouse, P.W., 2008. A Global Perspective on Renewable Energy Resources: Nasa's Prediction of Worldwide Energy Resources (Power) Project, in: Goswami, D.Y., Zhao, Y. (Eds.), Proceedings of ISES World Congress 2007 (Vol. I – Vol. V). Springer Berlin Heidelberg, Berlin, Heidelberg, pp. 2636–2640. https://doi.org/10.1007/978-3-540-75997-3_532

Figures

Figure 1

Map of Weather Measurement Sites and Agro-Ecological Zones

This color map of West Africa displays the geographic locations of the twenty weather measurement sites used in the study, overlaid on a representation of global agro-ecological zones as defined by the FAO and IIASA. Each site is indicated by a dot symbol. The color legend for the agro-ecological zones (AEZ) is provided to differentiate between the zones.

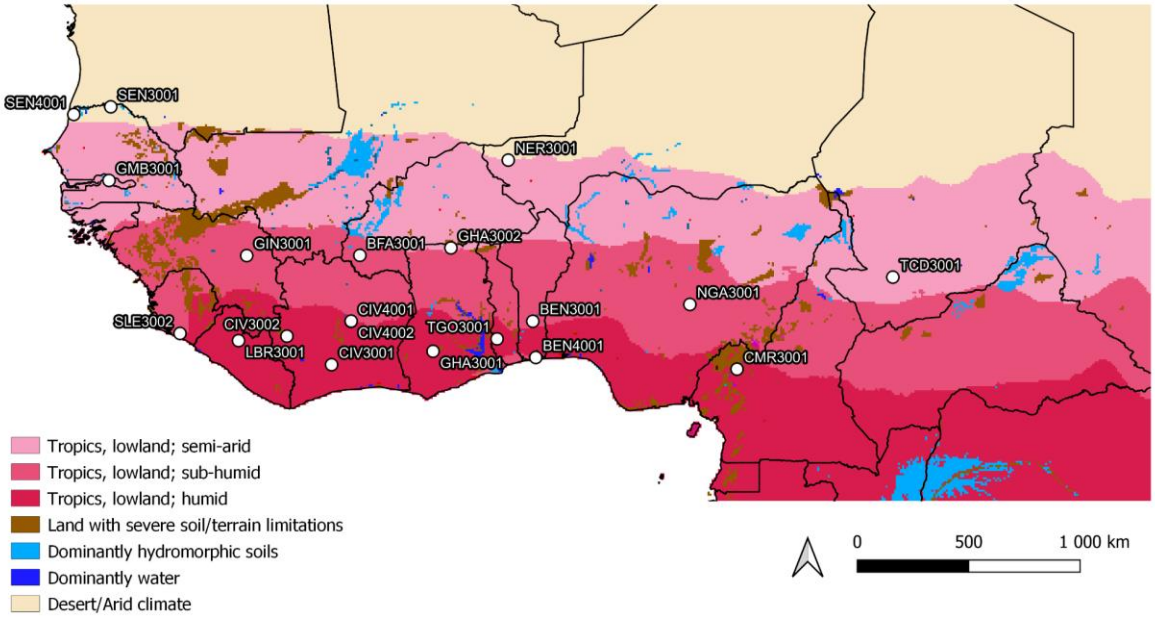

Figure 2

Surface Occupancy Histogram of AEZ

This histogram illustrates the distribution of surface occupancy percentages for the various Agro-Ecological Zones (AEZ) within the study's geographic extent. Each bar represents the proportion of an AEZ relative to the total area considered.

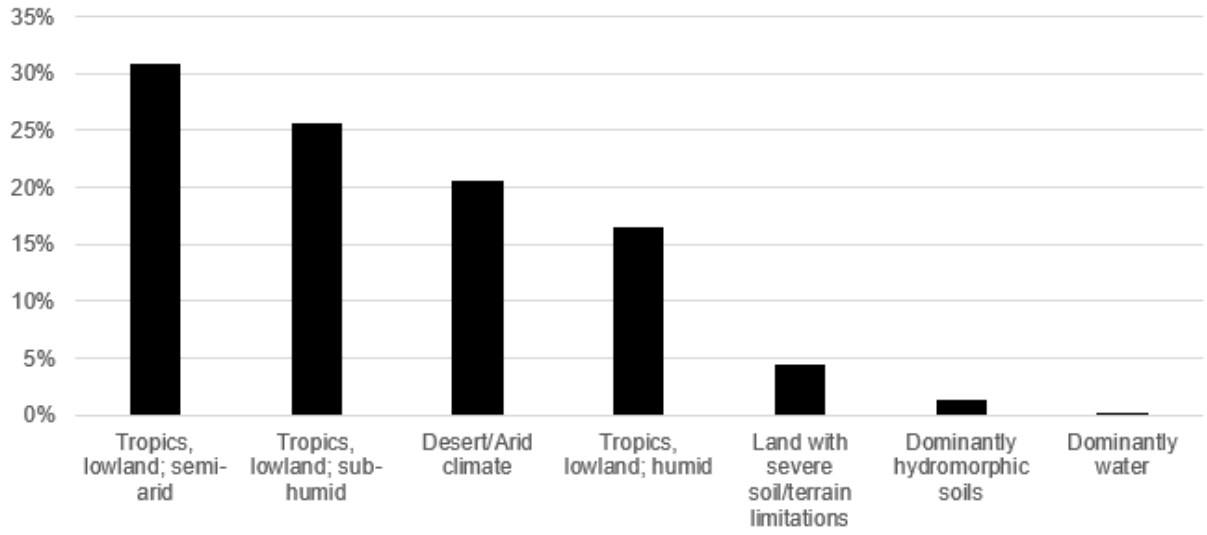
35%
30%
25%
20%
15%
10%
5%
0%
Tropics, lowland; semi-arid
Tropics, lowland; sub-humid
Desert/Arid climate
Tropics, lowland; humid
Land with severe soil/terrain limitations
Dominantly hydromorphic soils
Dominantly water

568

569

Tables

Table 1

In Situ Daily Data Collection Sites

This table enumerates the weather stations selected for the collection of daily in situ meteorological data. Detailed within are the geographical coordinates (latitude and longitude), altitude, country of location, data collection period, DOI for dataset reference, and the agro-ecological zones represented by each station.

Station name	Station code	Latitude	Longitude	Altitude (m)	Country	Measurement start	Measurement end	Dataset DOI	Agro-ecological zone
Glazoue	BEN3001	7.8800	2.2100	199	Benin	2012-07-05	2016-09-22	doi:10.7910/DVN/GVQYGG	Tropics, lowland; sub-humid
AfricaRice_Calavi	BEN4001	6.4200	2.3300	41	Benin	2012-03-19	2018-01-08	doi:10.7910/DVN/WTIMYZ	Tropics, lowland; humid
Farakoba	BFA3001	10.5400	-4.7600	319	Burkina Faso	2013-06-21	2018-03-08	doi:10.7910/DVN/TQX3L9	Tropics, lowland; sub-humid
Gagnoa_HUB	CIV3001	6.1300	-5.9000	248	Ivory Coast	2015-07-25	2018-06-13	doi:10.7910/DVN/A6SGP3	Tropics, lowland; humid
Man	CIV3002	7.2800	-7.7000	376	Ivory Coast	2012-07-21	2019-05-31	doi:10.7910/DVN/DQXCJC	Tropics, lowland; humid
Mbe_Low	CIV4001	7.8744	-5.1138	273	Ivory	2014-10-	2020-12-	doi:10.79	Tropics,

land					Coast	03	31	10/DVN/HVKBPL	lowland; humid
Mbe_Upland	CIV4002	7.8856	-5.1123	303	Ivory Coast	2014-10-10	2018-08-05	doi:10.7910/DVN/2C7XKY	Tropics, lowland; humid
Ndop	CMR3001	5.9500	10.4400	1185	Cameroon	2012-08-03	2015-06-24	doi:10.7910/DVN/ZSP7NQ	Land with severe soil/terrain limitations
Gimbi	COD3001	-5.2200	13.2700	364	Democratic Rep. Congo	2013-08-03	2014-02-01	doi:10.7910/DVN/IXPDM3	Tropics, highland; sub-humid
Kumasi	GHA3001	6.6700	-1.8100	236	Ghana	2012-06-23	2016-04-20	doi:10.7910/DVN/EUPQPZ	Tropics, lowland; humid
Navrongo	GHA3002	10.8400	-1.0900	173	Ghana	2013-05-14	2014-05-17	doi:10.7910/DVN/H5MX3J	Tropics, lowland; semi-arid
Kankan	GIN3001	10.5300	-9.3200	432	Guinea	2013-11-09	2016-03-16	doi:10.7910/DVN/6PHUPC	Tropics, lowland; sub-humid
Central_River	GMB3001	13.5600	-14.8700	41	Gambia	2013-03-07	2020-03-02	10.7910/DVN/ZLHPFP	Tropics, lowland; semi-arid
Cari	LBR3001	7.1000	-9.6500	273	Liberia	2015-10-08	2018-02-21	doi:10.7910/DVN/MJQVZO	Tropics, lowland; humid

Tillabery_HUB	NER3001	14.3800	1.2200	234	Niger	2012-07-29	2015-07-03	doi:10.7910/DVN/Q6ZDBV	Tropics, lowland; semi-arid
Lafia	NGA3001	8.5600	8.5400	150	Nigeria	2012-08-09	2018-02-25	doi:10.7910/DVN/8ERRWL	Tropics, lowland; sub-humid
Fanaye	SEN3001	16.5300	-14.8000	11	Senegal	2013-02-06	2020-12-31	doi:10.7910/DVN/9HVYWP	Desert/Arid climate
Ndiaye	SEN4001	16.2200	-16.2900	13	Senegal	2013-02-01	2019-12-14	doi:10.7910/DVN/HTLG35	Land with ample irrigated soils
Tormabum	SLE3002	7.3900	-12.0100	9	Sierra Leone	2014-05-28	2016-05-01	doi:10.7910/DVN/VWGJHE	Tropics, lowland; sub-humid
Tandjile_East	TCD3001	9.6600	16.7200	345	Chad	2013-06-07	2013-07-03	doi:10.7910/DVN/WKP6HR	Tropics, lowland; humid
Adeta	TGO3001	7.1700	0.7700	295	Togo	2013-04-04	2015-12-05	doi:10.7910/DVN/0SQFGQ	Tropics, lowland; humid

577

Table 2

Dataset Durations for Model Development

Summary of dataset lengths for ground weather observations, detailing the periods utilised for the training, validation, and testing of XGB models.

station code	on-site observations interval		subset duration (days)		
	start	end	train set	validation set	test set
BEN3001	2012-07-05	2016-09-22	10048	365	1540
BEN4001	2012-03-19	2018-01-08	9940	365	2121
BFA3001	2013-06-21	2018-03-08	10399	365	1721
CIV3001	2015-06-25	2018-06-13	11133	365	1084
CIV3002	2012-07-21	2019-05-31	10064	365	2505
CIV4001	2014-10-03	2020-12-31	10868	365	2281
CIV4002	2014-10-10	2018-10-05	10875	365	1456
CMR3001	2012-08-03	2015-06-24	10077	365	1055
COD3001	2013-08-03	2014-02-01	10442	365	182
GHA3001	2012-06-23	2016-04-20	10036	365	1397
GHA3002	2013-05-14	2014-05-17	10361	365	368
GIN3001	2013-11-09	2016-03-16	10540	365	858
GMB3001	2013-03-07	2020-03-07	10293	365	2557
LBR3001	2015-10-08	2018-02-21	11238	365	867
NER3001	2012-01-01	2015-07-03	9862	365	1279
NGA3001	2012-01-01	2018-02-25	9862	365	2247
SEN3001	2013-01-01	2020-12-31	10228	365	2921
SEN4001	2013-02-01	2019-12-31	10259	365	2524
SLE3002	2014-01-01	2016-06-22	10593	365	903
TCD3001	2013-01-12	2013-07-03	10239	365	172
TGO3001	2013-01-01	2015-12-05	10228	365	1068
		average	*10361*		*1481*

Table 3

Training Features for XGB Model Classes

This table specifies the combinations of meteorological variables used to train the eleven distinct XGB model classes, with each variable corresponding to data typically collected by standard meteorological instruments. X indicates the correspondence between the set of variables and the minimum set of sensors needed to measure these variables on site

model alias	Features used for training	maximum–minimum thermometer	temperature data logger	rain gauge	anemometer	hygrometer	pyranometer
M1	TMIN, TMAX	x					
M2	TEMP, TMIN, TMAX		x				
M3	TMIN, TMAX, RAIN	x		x			
M4	TEMP, TMIN, TMAX, RAIN		x	x			
M5	TEMP, TMIN, TMAX, RAIN, WIND		x	x	x		
M6	TEMP, TMIN, TMAX, RAIN, VAP		x	x		x	
M7	TEMP, TMIN, TMAX, RAIN, IRRAD		x	x			x
M8	TEMP, TMIN, TMAX, RAIN, WIND, VAP		x	x	x	x	
M9	TEMP, TMIN, TMAX, RAIN, WIND, IRRAD		x	x	x		x
M10	TEMP, TMIN, TMAX, RAIN, VAP, IRRAD		x	x		x	x
M11	TEMP, TMIN, TMAX, RAIN, WIND, VAP, IRRAD		x	x	x	x	x

Table 4

Empirical methods used for ET_0 estimations.

ET_0 reference evapotranspiration (mm); u2 represents the wind speed measured at 2 m from the ground (ms^{-1}); (es—ea) vapour saturation deficit (kPa); Ta is the average air temperature (°C); Tmax—maximum temperature (°C); Tmin—minimum temperature (°C); Rs is the short wavelength solar radiation (MJ $m^{-2}d^{-1}$); φ represents the latitude of the station in radian degree, and λ is the latent heat of vaporisation ($MJ.m^{-2}d^{-1}$).

Category	Reference	Formula
Aerodynamic	Dalton (Dalton, J, 1802)	$ET_0 = (0.3648 + 0.07223u2)(es - ea)$
	Trabert (Trabert, W, 1896)	$ET_0 = 0.3075\sqrt{u2}(es - ea)$
	Penman (Penman, H. L., 1963)	$ET_0 = 0.35(1 + 0.24u2)(es - ea)$
	Rohwer (Rohwer, Carl, 1931)	$ET_0 = 0.44(1 + 0.27u2)(es - ea)$
	Mahringer (Mahringer, 1970)	$ET_0 = 0.15072\sqrt{3.6}u2(es - ea)$
Temperature	Hargreaves (George H. Hargreaves and Zohrab A. Samani, 1985)	$ET_0 = 0.0135 \times 0.408Rs(Ta + 17.8)$
Radiation	Jensen & Haise (Jensen and Haise, 1963)	$ET_0 = 0.025(Ta - 3)Rs$
	Abtew (Abtew, 1996)	$ET_0 = 0.53\frac{Rs}{\lambda}$
	Oudin (Oudin, Ludovic, 2004)	$ET_0 = Rs \times \frac{Ta + 5}{100}$
	Irmak (a) (Irmak et al., 2003a, 2003b)	$ET_0 = 0.149Rs + 0.079Ta - 0.611$
	Irmak (b) (Irmak et al., 2003a, 2003b)	$ET_0 = 0.174Rs + 0.353Ta - 0.642$
	Irmak (c) (Irmak et al., 2003a, 2003b)	$ET_0 = 0.156Rs - 0.0112Tmax + 0.0733Tmin - 0.478$

Combinatory	Valiantzas (a) (Valiantzas, 2013)	$ET_0 = (0.0393Rs \times \sqrt{Ta + 9.5}) - 0.19Rs^{0.6}\varphi^{0.15} + 0.048(Ta + 20)(1 - \frac{Hr}{100})u2^{0.7}$
	Valiantzas (b) (Valiantzas, 2013)	$ET_0 = (0.0393Rs \times \sqrt{Ta + 9.5}) - 0.19Rs^{0.6}\varphi^{0.15} + 0.078(Ta + 20)(1 - \frac{Hr}{100})$
	Valiantzas (c) (Valiantzas, 2013)	$ET_0 = (0.0393Rs \times \sqrt{Ta + 9.5}) - 0.19Rs^{0.6}\varphi^{0.15} + 0.0061(Ta + 20)(1.12Ta - Tmin - 2)^{0.7}$

597

598

Table 5

Validation Metrics for XGB Models

This table provides the root mean square error (RMSE) and coefficient of determination (R2) obtained from the validation sets used in the training of the eleven XGB model classes.

	station	model class										
		M1	M2	M3	M4	M5	M6	M7	M8	M9	M10	M11
RMSE (mm)	BEN3001	0,43	0,43	0,42	0,42	0,42	0,41	0,20	0,41	0,15	0,16	0,06
	BEN4001	0,50	0,48	0,47	0,47	0,47	0,46	0,14	0,47	0,12	0,12	0,06
	BFA3001	0,77	0,78	0,74	0,76	0,49	0,68	0,61	0,48	0,29	0,51	0,10
	CIV3001	0,41	0,41	0,40	0,41	0,40	0,42	0,13	0,41	0,10	0,10	0,06
	CIV3002	0,38	0,38	0,38	0,38	0,37	0,38	0,15	0,37	0,12	0,12	0,07
	CIV4001	0,55	0,56	0,55	0,56	0,50	0,53	0,35	0,48	0,25	0,32	0,09
	CIV4002	0,55	0,56	0,55	0,56	0,50	0,53	0,35	0,48	0,25	0,32	0,09
	CMR3001	0,41	0,42	0,39	0,39	0,40	0,37	0,12	0,38	0,12	0,09	0,05
	COD3001	0,69	0,67	0,70	0,68	0,67	0,66	0,06	0,66	0,06	0,06	0,04
	GHA3001	0,43	0,44	0,43	0,44	0,43	0,42	0,24	0,42	0,19	0,20	0,07
	GHA3002	0,81	0,82	0,81	0,83	0,53	0,72	0,67	0,51	0,34	0,54	0,12
	GIN3001	0,71	0,72	0,71	0,73	0,50	0,69	0,58	0,50	0,33	0,53	0,11
	GMB3001	0,96	0,94	0,95	0,96	0,57	0,81	0,90	0,50	0,46	0,74	0,13
	LBR3001	0,40	0,40	0,39	0,40	0,38	0,39	0,11	0,38	0,10	0,10	0,06
	NER3001	1,14	1,14	1,13	1,14	0,57	0,98	1,09	0,50	0,48	0,95	0,16
	NGA3001	0,75	0,75	0,76	0,76	0,53	0,63	0,66	0,50	0,34	0,43	0,12
	SEN3001	1,44	1,45	1,43	1,45	0,61	1,22	1,33	0,48	0,53	1,09	0,19
	SEN4001	1,09	1,08	1,07	1,06	0,63	0,90	1,03	0,45	0,62	0,75	0,19
	SLE3002	0,55	0,55	0,54	0,55	0,53	0,55	0,10	0,54	0,09	0,09	0,06
	TCD3001	0,97	0,95	0,98	0,97	0,53	0,79	0,83	0,53	0,31	0,63	0,11
	TGO3001	0,43	0,43	0,43	0,43	0,43	0,42	0,18	0,42	0,14	0,17	0,07
	mean	*0,68*	*0,68*	*0,68*	*0,68*	*0,50*	*0,62*	*0,47*	*0,47*	*0,26*	*0,38*	*0,09*
	median	*0,55*	*0,56*	*0,55*	*0,56*	*0,50*	*0,55*	*0,35*	*0,48*	*0,25*	*0,32*	*0,09*
R2	BEN3001	0,58	0,57	0,60	0,59	0,60	0,62	0,91	0,62	0,95	0,94	0,99
	BEN4001	0,43	0,46	0,49	0,49	0,50	0,51	0,96	0,50	0,97	0,97	0,99
	BFA3001	0,76	0,76	0,78	0,77	0,90	0,82	0,85	0,91	0,97	0,90	1,00
	CIV3001	0,33	0,32	0,34	0,32	0,35	0,28	0,93	0,31	0,96	0,96	0,99
	CIV3002	0,61	0,62	0,61	0,62	0,62	0,62	0,94	0,62	0,96	0,96	0,99
	CIV4001	0,75	0,74	0,75	0,74	0,80	0,77	0,90	0,81	0,95	0,91	0,99
	CIV4002	0,75	0,74	0,74	0,73	0,79	0,77	0,90	0,81	0,95	0,91	0,99
	CMR3001	0,68	0,67	0,72	0,71	0,70	0,74	0,97	0,73	0,97	0,98	1,00
	COD3001	0,11	0,15	0,09	0,14	0,16	0,18	0,99	0,19	0,99	0,99	1,00
	GHA3001	0,72	0,71	0,72	0,71	0,72	0,73	0,91	0,73	0,95	0,94	0,99
	GHA3002	0,78	0,77	0,78	0,77	0,91	0,83	0,85	0,91	0,96	0,90	1,00
	GIN3001	0,82	0,82	0,82	0,81	0,91	0,83	0,88	0,91	0,96	0,90	1,00
	GMB3001	0,81	0,82	0,81	0,81	0,93	0,86	0,83	0,95	0,96	0,89	1,00
	LBR3001	0,42	0,42	0,44	0,42	0,47	0,44	0,96	0,48	0,97	0,96	0,99
	NER3001	0,57	0,57	0,58	0,57	0,89	0,68	0,61	0,92	0,92	0,70	0,99
	NGA3001	0,82	0,82	0,82	0,82	0,91	0,88	0,87	0,92	0,96	0,94	1,00
	SEN3001	0,55	0,54	0,55	0,54	0,92	0,67	0,61	0,95	0,94	0,74	0,99
	SEN4001	0,59	0,59	0,60	0,61	0,86	0,72	0,64	0,93	0,86	0,80	0,99
	SLE3002	0,54	0,54	0,55	0,54	0,57	0,54	0,99	0,56	0,99	0,99	0,99
	TCD3001	0,74	0,75	0,73	0,74	0,92	0,83	0,81	0,92	0,97	0,89	1,00
	TGO3001	0,65	0,65	0,65	0,64	0,65	0,66	0,94	0,66	0,96	0,95	0,99
	mean	*0,62*	*0,62*	*0,63*	*0,62*	*0,72*	*0,66*	*0,87*	*0,73*	*0,96*	*0,91*	*0,99*
	median	*0,65*	*0,65*	*0,65*	*0,64*	*0,79*	*0,72*	*0,90*	*0,81*	*0,96*	*0,94*	*0,99*

603

604

Table 6

Performance Comparison of XGB and Empirical ET0 Formulas

This table presents the average metrics from the comparison between XGB model estimations and those calculated using empirical ET_0 formulas against the standard ET_0-PM-GT values. Metrics include RMSE and R^2 values for each model and formula.

	station	model class											empirical methods														
		M1	M2	M3	M4	M5	M6	M7	M8	M9	M10	M11	abtew	dalton	hargreaves	irmak-a	irmak-b	irmak-c	jensen-haise	mahringer	oudin	penman	rohwer	trabert	valiantzas-a	valiantzas-b	valiantzas-c
RMSE (mm)	BEN3001	1,16	1,17	1,25	1,25	1,20	1,09	1,49	0,95	1,51	0,93	0,84	1,81	4,90	1,65	1,58	3,16	2,10	4,43	4,93	1,08	4,89	4,80	4,96	1,76	1,70	1,61
	BEN4001	1,52	1,48	1,61	1,54	1,54	1,20	1,64	1,09	1,68	1,16	1,23	1,80	5,14	1,66	1,62	3,13	1,99	5,26	5,11	1,37	5,14	5,19	5,13	1,94	1,93	1,75
	BFA3001	2,08	2,05	2,33	2,26	1,21	4,27	2,02	2,08	1,10	3,59	0,99	0,81	4,06	0,79	0,65	1,97	1,16	6,27	4,17	1,54	4,06	3,97	4,15	0,78	0,97	0,80
	CIV3001	0,59	0,61	0,61	0,64	0,58	0,56	0,83	0,49	0,85	0,78	0,70	0,97	4,07	0,92	0,78	2,21	1,22	5,16	4,17	1,14	4,07	3,99	4,15	1,12	0,98	0,89
	CIV3002	0,55	0,55	0,58	0,55	0,53	0,81	0,61	0,80	0,61	0,44	0,45	0,82	3,60	0,80	0,52	1,99	1,04	4,34	3,71	0,94	3,60	3,53	3,69	0,92	0,81	0,72
	CIV4001	1,31	1,31	1,30	1,27	1,17	2,21	1,39	1,45	1,42	1,63	0,81	1,60	4,49	1,56	1,44	2,84	1,95	4,00	4,55	1,17	4,49	4,40	4,56	1,67	1,57	1,49
	CIV4002	0,91	0,92	0,93	0,91	0,82	2,38	0,99	1,58	1,05	1,93	0,63	1,18	4,30	1,10	1,01	2,44	1,52	5,08	4,39	1,13	4,30	4,22	4,39	1,24	1,15	1,05
	CMR3001	0,66	0,65	0,65	0,59	0,56	0,79	0,72	0,69	0,76	0,46	0,51	0,88	4,26	1,11	1,10	2,23	1,68	3,19	4,32	0,69	4,26	4,18	4,33	1,08	0,91	0,94
	COD3001	2,03	2,06	2,09	2,12	2,19	2,54	2,62	2,42	2,68	2,77	2,82	2,33	4,66	2,44	2,04	3,46	2,46	2,53	4,67	2,02	4,66	4,59	4,70	2,48	2,42	2,32
	GHA3001	1,26	1,23	1,26	1,17	0,93	2,36	0,89	1,86	0,74	1,89	0,86	0,57	3,38	0,60	0,44	1,65	0,72	5,18	3,53	1,27	3,38	3,31	3,49	0,71	0,66	0,63
	GHA3002	1,63	1,61	1,62	1,60	1,22	3,57	1,63	1,47	1,24	3,24	0,70	1,60	5,33	1,34	1,54	3,05	2,11	7,12	5,35	1,54	5,32	5,17	5,43	1,16	1,28	1,36
	GIN3001	1,41	1,43	1,44	1,44	1,01	2,89	1,28	1,58	0,98	2,30	0,57	1,36	4,71	1,24	1,26	2,69	1,90	5,25	4,77	1,10	4,71	4,61	4,79	1,11	1,04	1,12
	GMB3001	2,16	2,07	2,10	2,03	1,53	3,62	2,00	1,82	1,49	3,59	1,07	2,60	6,62	2,20	2,65	4,06	3,25	7,35	6,54	1,83	6,62	6,49	6,68	1,53	1,95	2,22
	LBR3001	1,01	1,03	1,01	1,03	0,98	0,70	1,41	0,64	1,40	0,77	0,95	1,48	4,77	1,43	1,33	2,82	1,80	4,32	4,79	1,02	4,77	4,72	4,80	1,28	1,60	1,43
	NER3001	2,24	2,11	2,22	2,07	1,14	2,74	2,10	1,20	1,01	2,43	0,65	1,96	6,26	1,83	2,10	3,43	2,67	8,16	6,23	2,13	6,25	6,16	6,31	1,16	1,54	1,85
	NGA3001	2,03	2,10	2,04	2,15	1,58	5,14	1,69	3,07	1,18	4,46	1,67	1,25	4,04	1,11	0,87	2,40	1,41	5,38	4,15	1,31	4,04	3,95	4,13	1,01	1,05	0,99
	SEN3001	3,33	3,24	3,27	3,17	1,59	4,32	2,65	2,02	1,33	3,69	1,15	2,54	6,03	2,27	2,48	3,86	3,14	6,25	5,98	1,88	6,02	5,90	6,10	1,65	1,96	2,18
	SEN4001	2,61	2,61	2,54	2,53	2,18	2,94	2,40	2,17	2,04	3,43	1,62	2,63	6,48	2,56	2,87	4,03	3,34	5,76	6,38	2,08	6,47	6,35	6,54	2,08	2,44	2,64
	SLE3002	0,68	0,64	0,69	0,64	0,66	0,69	1,19	0,66	1,21	1,01	1,03	1,57	4,11	1,43	1,05	2,72	1,57	3,51	4,16	0,98	4,11	4,07	4,15	1,14	1,52	1,30
	TCD3001	2,07	2,07	1,88	1,90	1,39	1,84	2,00	0,33	1,46	1,57	0,90	2,72	6,69	2,42	2,72	4,32	3,28	6,12	6,58	1,63	6,68	6,54	6,75	2,18	2,31	2,49
	TGO3001	0,89	0,87	0,88	0,82	0,75	1,68	0,75	1,29	0,76	1,28	0,71	0,77	3,76	0,81	0,67	1,75	0,90	5,80	3,88	1,52	3,76	3,68	3,85	0,80	0,81	0,80
	mean	*1,53*	*1,51*	*1,54*	*1,51*	*1,18*	*2,30*	*1,54*	*1,41*	*1,26*	*2,06*	*0,99*	*1,58*	*4,84*	*1,49*	*1,46*	*2,87*	*1,96*	*5,26*	*4,87*	*1,40*	*4,84*	*4,75*	*4,91*	*1,37*	*1,46*	*1,46*
	median	*1,41*	*1,43*	*1,44*	*1,44*	*1,17*	*2,36*	*1,49*	*1,45*	*1,21*	*1,83*	*0,86*	*1,57*	*4,66*	*1,43*	*1,33*	*2,82*	*1,90*	*5,25*	*4,67*	*1,31*	*4,66*	*4,59*	*4,70*	*1,16*	*1,52*	*1,36*
corr coeff	BEN3001	0,43	0,44	0,41	0,42	0,50	0,48	0,56	0,57	0,65	0,62	0,76	0,58	0,60	0,62	0,62	0,58	0,66	0,63	0,88	0,62	0,62	0,64	0,76	0,63	0,44	0,55
	BEN4001	0,03	0,10	0,04	0,11	0,28	0,20	0,43	0,45	0,51	0,49	0,65	0,56	-0,20	0,56	0,55	0,56	0,59	0,55	-0,12	0,56	-0,19	-0,19	-0,17	0,53	0,39	0,50
	BFA3001	0,24	0,24	0,38	0,39	0,50	0,52	0,43	0,61	0,56	0,61	0,69	0,52	0,31	0,62	0,64	0,53	0,62	0,67	0,70	0,65	0,33	0,34	0,54	0,71	0,58	0,58
	CIV3001	0,53	0,54	0,52	0,54	0,66	0,55	0,58	0,69	0,69	0,60	0,75	0,52	0,48	0,56	0,57	0,53	0,57	0,59	0,85	0,58	0,50	0,52	0,71	0,62	0,53	0,54
	CIV3002	0,60	0,59	0,59	0,59	0,66	0,61	0,78	0,66	0,85	0,81	0,88	0,71	0,68	0,75	0,78	0,72	0,74	0,77	0,81	0,76	0,69	0,70	0,76	0,78	0,66	0,75
	CIV4001	0,13	0,15	0,13	0,19	0,35	0,25	0,35	0,53	0,51	0,47	0,68	0,50	0,27	0,55	0,57	0,51	0,61	0,59	0,85	0,57	0,31	0,34	0,64	0,61	0,44	0,48
	CIV4002	0,44	0,45	0,44	0,47	0,54	0,57	0,54	0,67	0,59	0,63	0,74	0,54	0,55	0,60	0,62	0,55	0,63	0,64	0,89	0,62	0,57	0,59	0,78	0,65	0,52	0,57
	CMR3001	0,66	0,69	0,64	0,71	0,73	0,80	0,78	0,84	0,82	0,84	0,90	0,69	0,68	0,75	0,76	0,69	0,66	0,80	0,90	0,78	0,70	0,71	0,81	0,84	0,77	0,78
	COD3001	0,17	0,18	0,08	0,07	0,17	0,27	0,61	0,23	0,61	0,62	0,61	0,60	0,59	0,60	0,61	0,60	0,59	0,60	0,79	0,60	0,61	0,62	0,69	0,67	0,62	0,62
	GHA3001	0,17	0,18	0,16	0,19	0,29	0,28	0,51	0,41	0,60	0,64	0,69	0,77	0,40	0,77	0,77	0,77	0,79	0,77	0,87	0,77	0,42	0,44	0,75	0,81	0,70	0,72
	GHA3002	0,22	0,23	0,28	0,29	0,46	0,52	0,37	0,62	0,54	0,57	0,83	0,44	0,53	0,53	0,53	0,44	0,55	0,58	0,81	0,55	0,55	0,57	0,68	0,67	0,50	0,48
	GIN3001	0,26	0,26	0,31	0,33	0,43	0,49	0,38	0,60	0,54	0,58	0,84	0,38	0,54	0,52	0,55	0,39	0,53	0,59	0,86	0,56	0,56	0,58	0,74	0,68	0,50	0,47
	GMB3001	0,42	0,47	0,47	0,51	0,72	0,66	0,54	0,79	0,74	0,70	0,92	0,51	0,53	0,59	0,60	0,52	0,60	0,63	0,81	0,61	0,56	0,58	0,69	0,78	0,55	0,56
	LBR3001	0,30	0,31	0,28	0,29	0,38	0,33	0,47	0,44	0,53	0,52	0,64	0,47	0,33	0,50	0,50	0,47	0,54	0,52	0,47	0,51	0,33	0,34	0,38	0,31	0,08	0,45
	NER3001	-0,19	-0,08	-0,17	-0,04	0,64	0,03	0,03	0,83	0,70	0,10	0,90	0,02	-0,03	0,03	0,02	0,02	0,13	0,03	0,55	0,03	0,01	0,03	0,18	0,62	0,18	-0,06
	NGA3001	0,33	0,29	0,33	0,32	0,34	0,48	0,40	0,47	0,47	0,60	0,61	0,44	0,35	0,50	0,54	0,44	0,51	0,54	0,61	0,52	0,36	0,37	0,48	0,68	0,51	0,50
	SEN3001	0,21	0,21	0,30	0,31	0,67	0,43	0,47	0,73	0,78	0,61	0,92	0,50	0,68	0,57	0,58	0,50	0,58	0,60	0,91	0,58	0,71	0,72	0,85	0,76	0,49	0,53
	SEN4001	0,07	0,07	0,11	0,12	0,32	0,20	0,23	0,39	0,41	0,39	0,77	0,39	0,72	0,41	0,40	0,39	0,41	0,39	0,94	0,40	0,75	0,77	0,89	0,78	0,42	0,37
	SLE3002	0,40	0,43	0,41	0,46	0,40	0,42	0,60	0,41	0,67	0,61	0,73	0,45	0,15	0,50	0,54	0,45	0,48	0,54	0,34	0,52	0,15	0,16	0,23	0,52	0,29	0,53
	TCD3001	0,72	0,69	0,64	0,59	0,96	0,59	0,60	0,96	0,93	0,59	0,90	0,55	0,83	0,56	0,56	0,55	0,53	0,57	0,95	0,57	0,84	0,85	0,88	0,73	0,63	0,58
	TGO3001	0,32	0,34	0,29	0,36	0,42	0,38	0,54	0,55	0,60	0,58	0,63	0,58	0,61	0,59	0,59	0,58	0,59	0,59	0,91	0,59	0,63	0,65	0,85	0,70	0,60	0,58
	mean	*0,31*	*0,32*	*0,32*	*0,34*	*0,50*	*0,43*	*0,49*	*0,59*	*0,63*	*0,58*	*0,76*	*0,51*	*0,46*	*0,56*	*0,57*	*0,51*	*0,57*	*0,58*	*0,74*	*0,57*	*0,48*	*0,49*	*0,63*	*0,67*	*0,50*	*0,53*
	median	*0,30*	*0,29*	*0,31*	*0,33*	*0,46*	*0,48*	*0,51*	*0,60*	*0,60*	*0,60*	*0,75*	*0,52*	*0,53*	*0,56*	*0,57*	*0,53*	*0,59*	*0,59*	*0,85*	*0,58*	*0,56*	*0,58*	*0,71*	*0,68*	*0,51*	*0,54*

Table 7

Taylor Diagram Analysis

Summary of the qualitative analysis based on Taylor diagrams for model performance across the 20 study sites.

	Tropics, lowland; sub-humid					Tropics, lowland; humid									Tropics, lowland; semi-arid			Desert/Arid climate	Land with severe soil / terrain limitations	Land with ample irrigated soils		
	BEN3001	BFA3001	GIN3001	NGA3001	SLE3002	BEN4001	CIV3001	CIV3002	CIV4001	CIV4002	GHA3001	LBR3001	TCD3001	TGO3001	GHA3002	GMB3001	NER3001	SEN3001	CMR3001	SEN4001	SUM	RANK
Dalton																					0	19
Trabert																					0	19
Penman																					0	19
Rohwer																					0	19
Mahringer															x						1	16
Hargreaves	x	x		x				x	x	x	x	x		x					x		7	3
Jansen-Haise																					0	19
Abtew								x	x		x			x					x		5	9
Oudin								x			x										2	13
Irmak-a	x	x		x		x		x	x	x	x	x		x					x		8	2
irmak-b						x		x	x		x			x							5	9
Irmak-c	x	x		x		x		x	x	x	x	x		x							7	3
Valiantzas-a	x	x		x			x	x	x	x	x			x					x		7	3
Valiantzas-b														x					x		2	13
Valiantzas-c				x				x			x			x					x		4	11
M1																					0	19
M2																					0	19
M3																			x		1	16
M4																					0	19
M5							x						x						x		3	12
M6																			x		1	16
M7														x					x		2	13
M8		x					x		x	x			x	x			x		x		7	3
M9	x				x		x	x				x	x	x					x		6	7
M10	x	x		x	x		x	x		x		x		x					x		6	7
M11	x	x	x	x	x	x	x	x	x	x		x	x	x	x	x	x	x	x		13	1

Supplementary figures

Figure S1

Taylor diagrams for comparison of our approach versus empirical methods

S1(a) Taylor diagram for station BEN3001

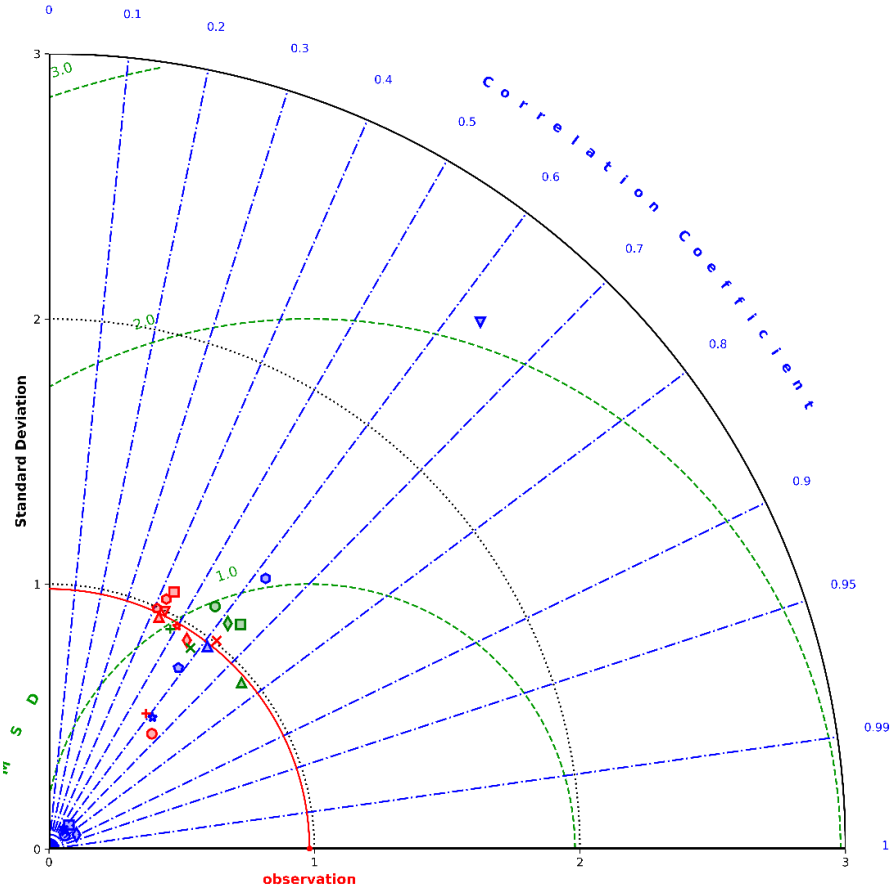

S1(b) Taylor diagram for station BEN4001

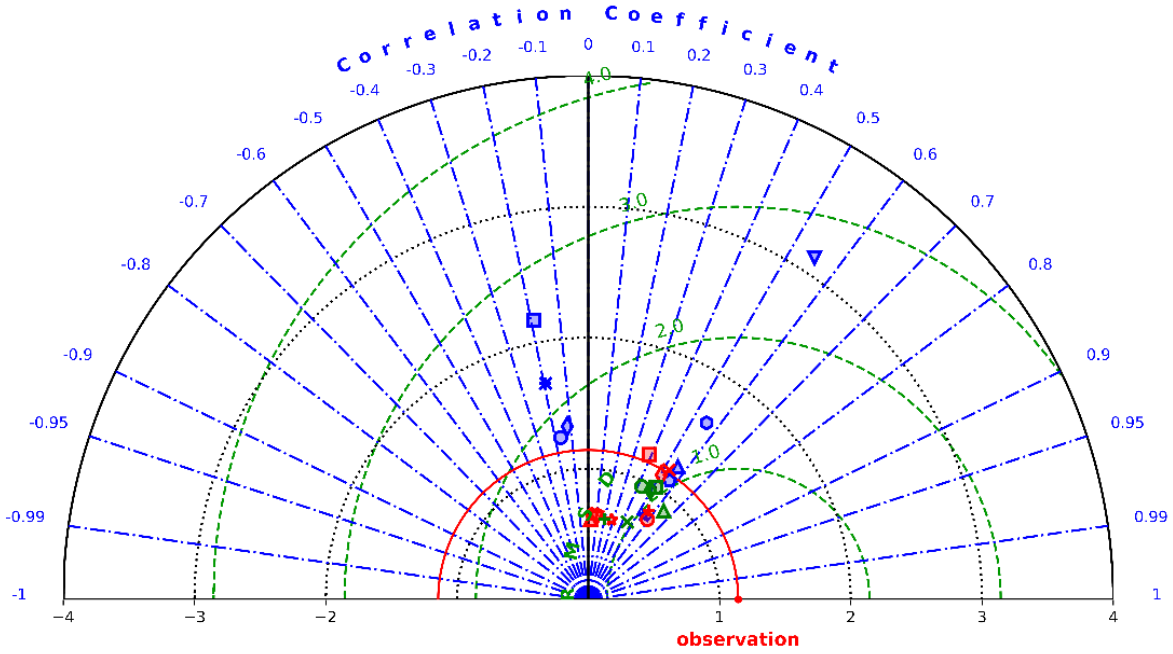

S1(c) Taylor diagram for station BFA3001

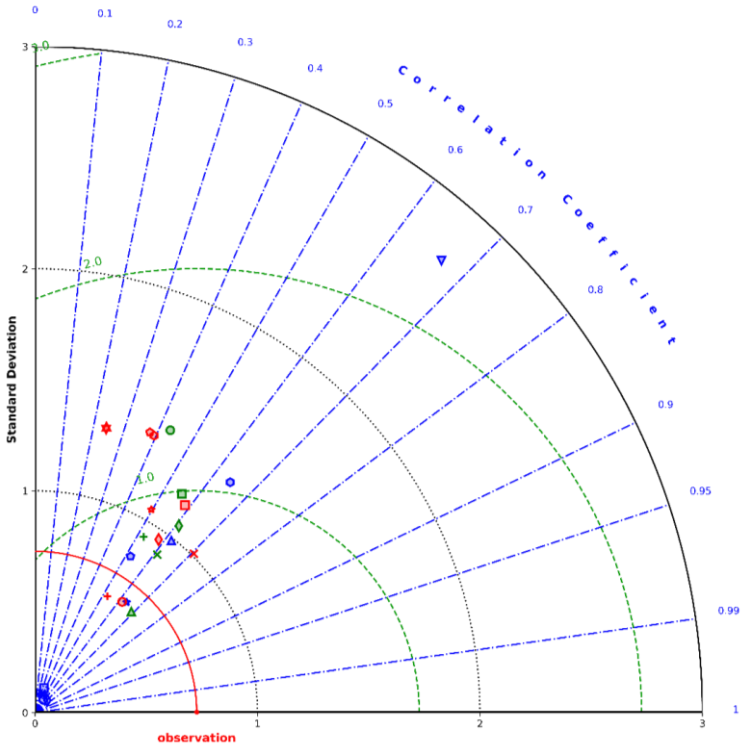

S1(d) Taylor diagram for station CIV3001

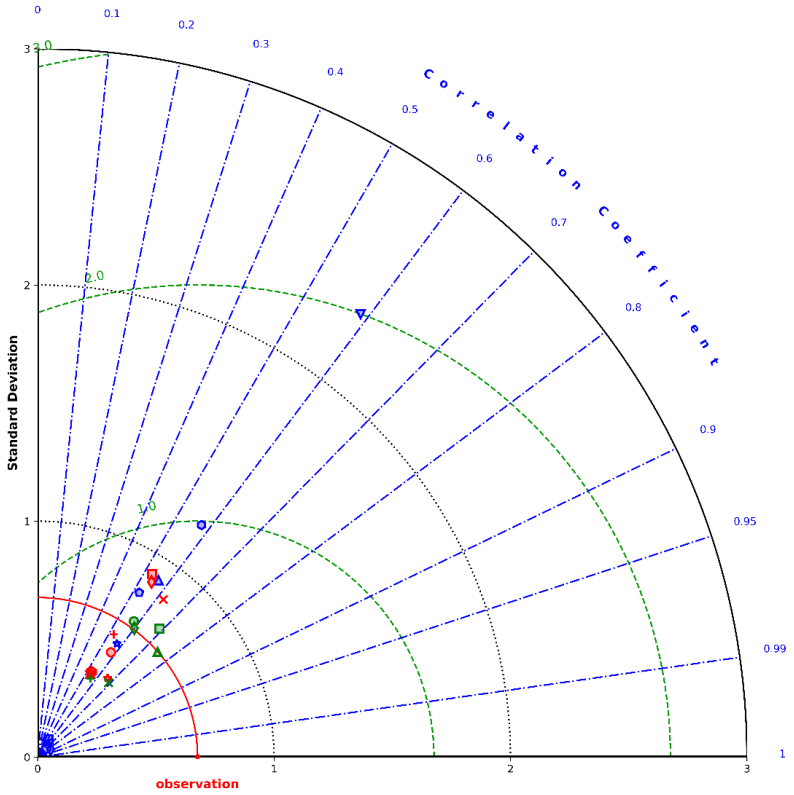

S1(e) Taylor diagram for station CIV3002

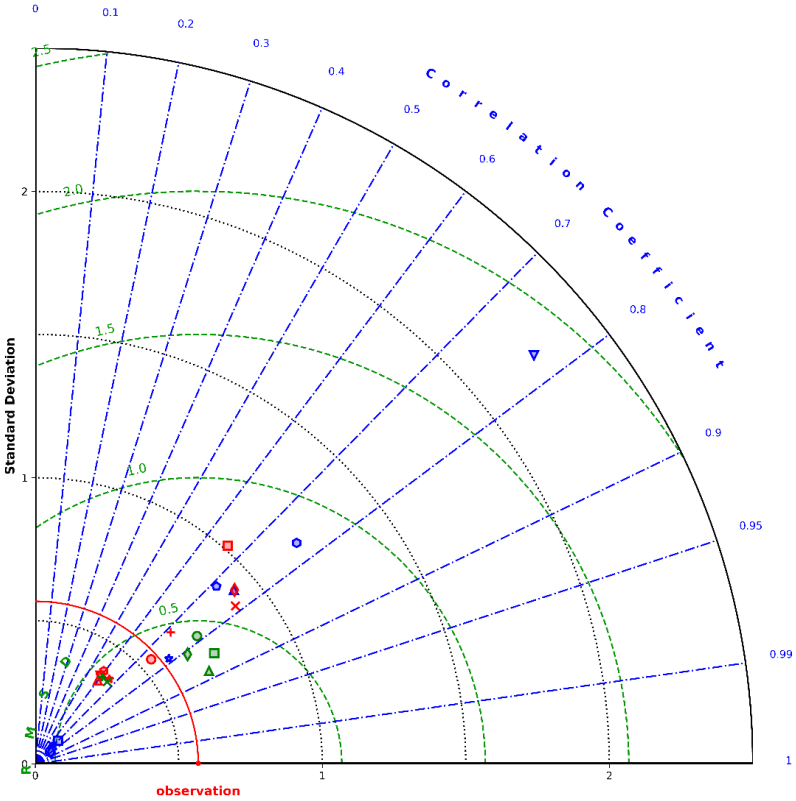

S1(f) Taylor diagram for station CIV4001

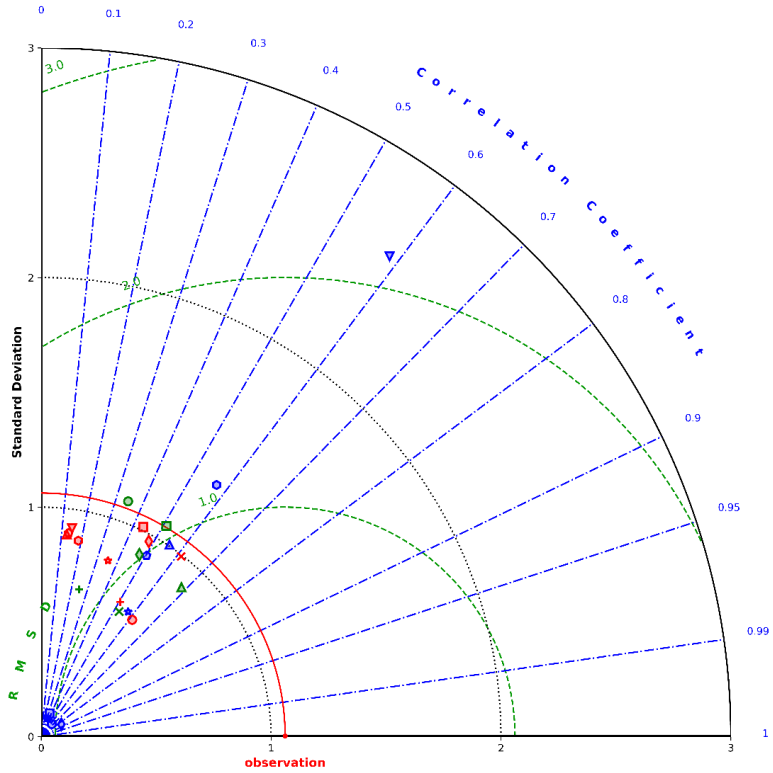

S1(g) Taylor diagram for station CIV4002

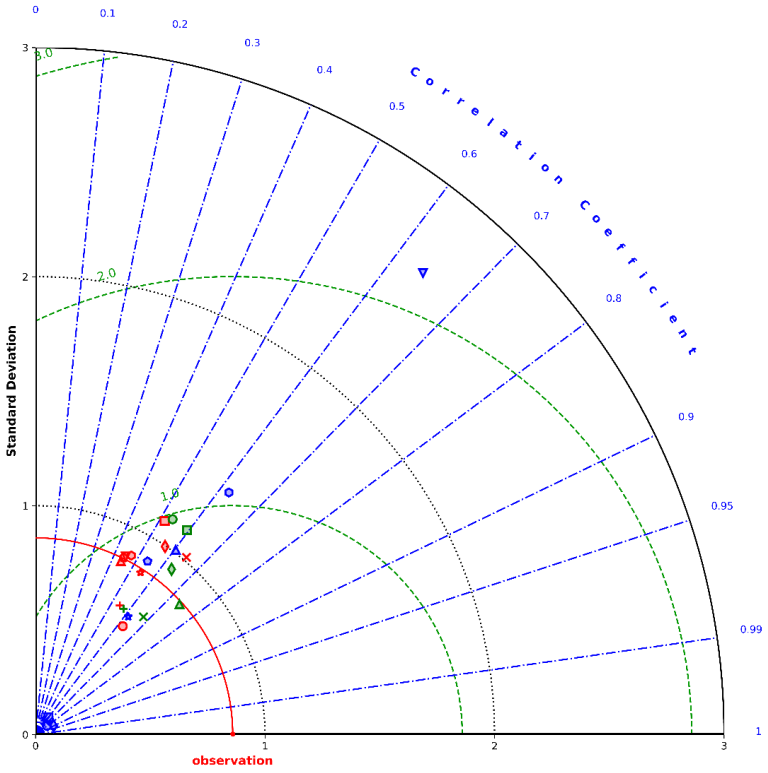

S1(h) Taylor diagram for station CMR3001

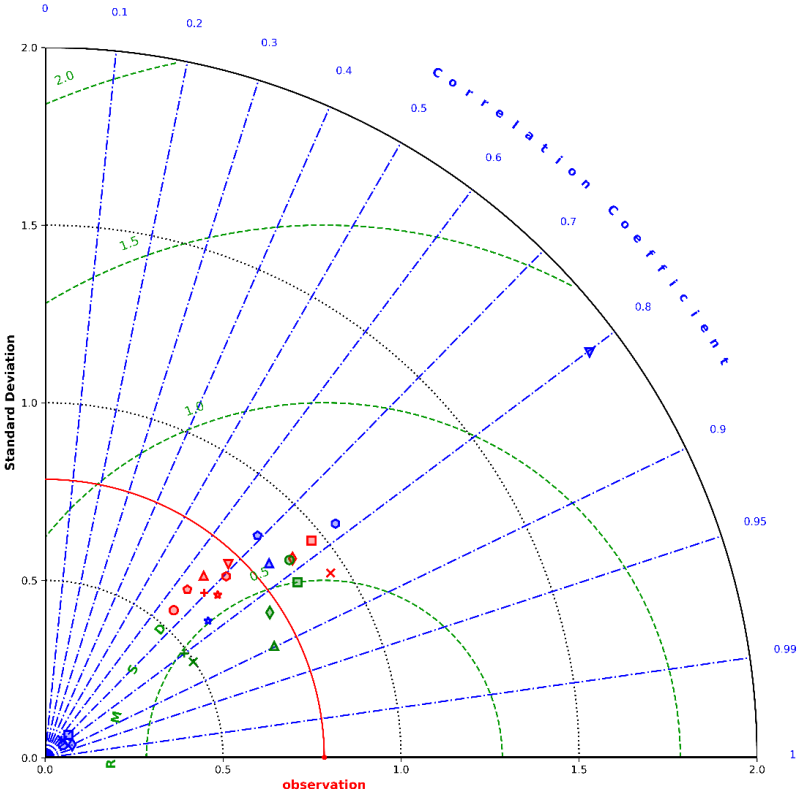

S1(i) Taylor diagram for station COD3001

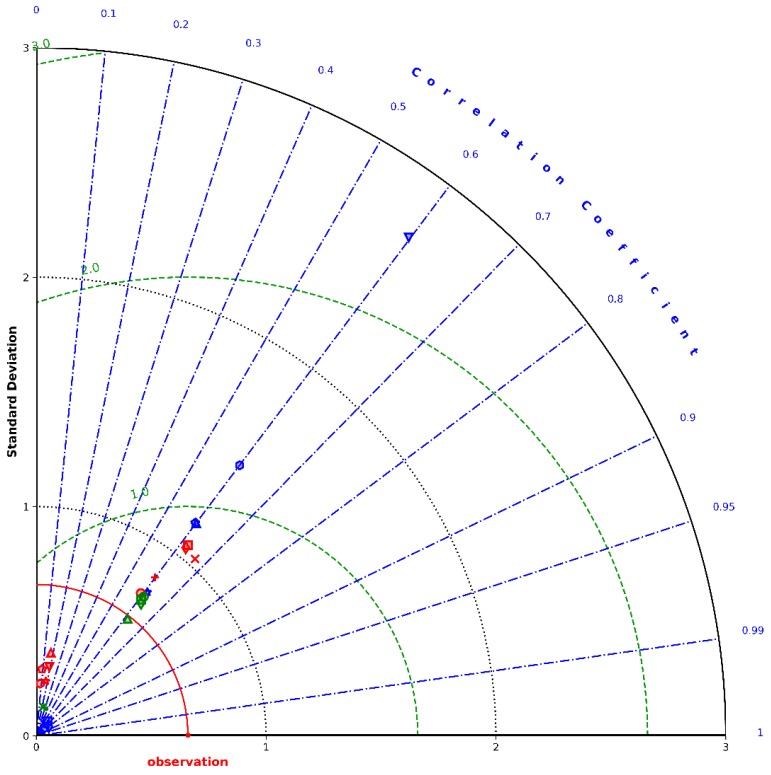

S1(j) Taylor diagram for station GHA3001

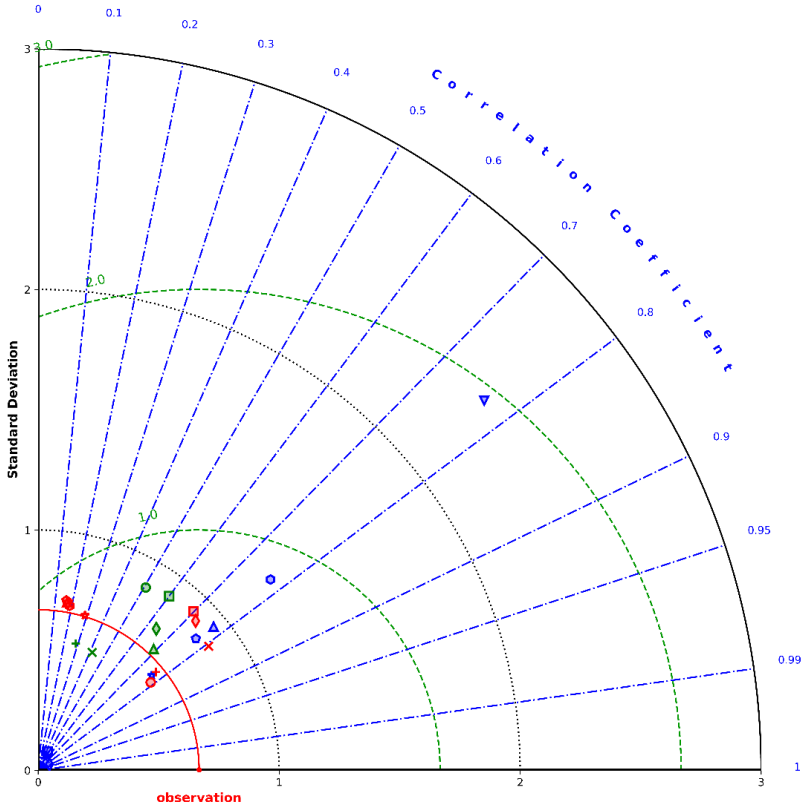

S1(k) Taylor diagram for station GHA3002

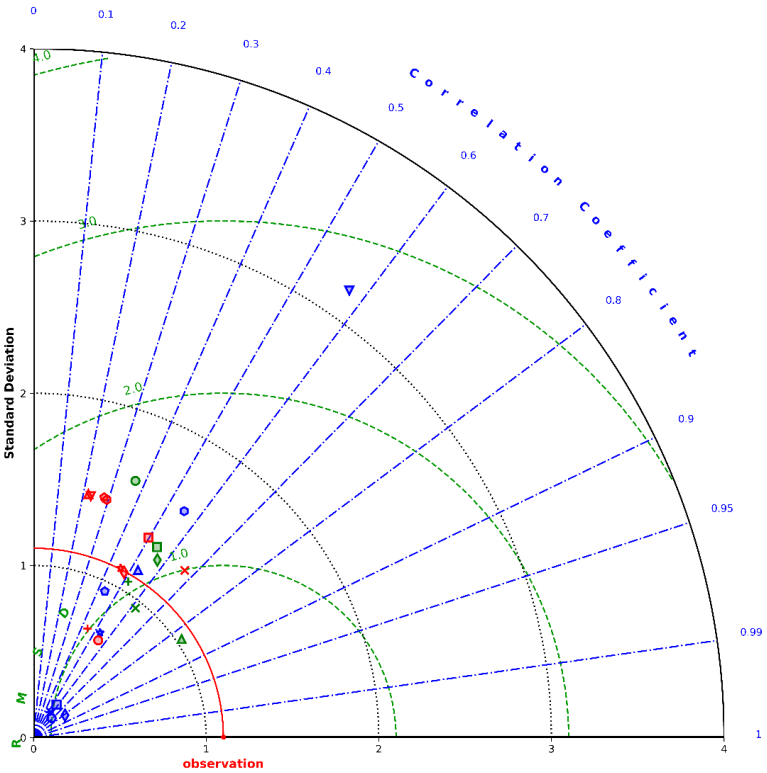

S1(l) Taylor diagram for station GIN3001

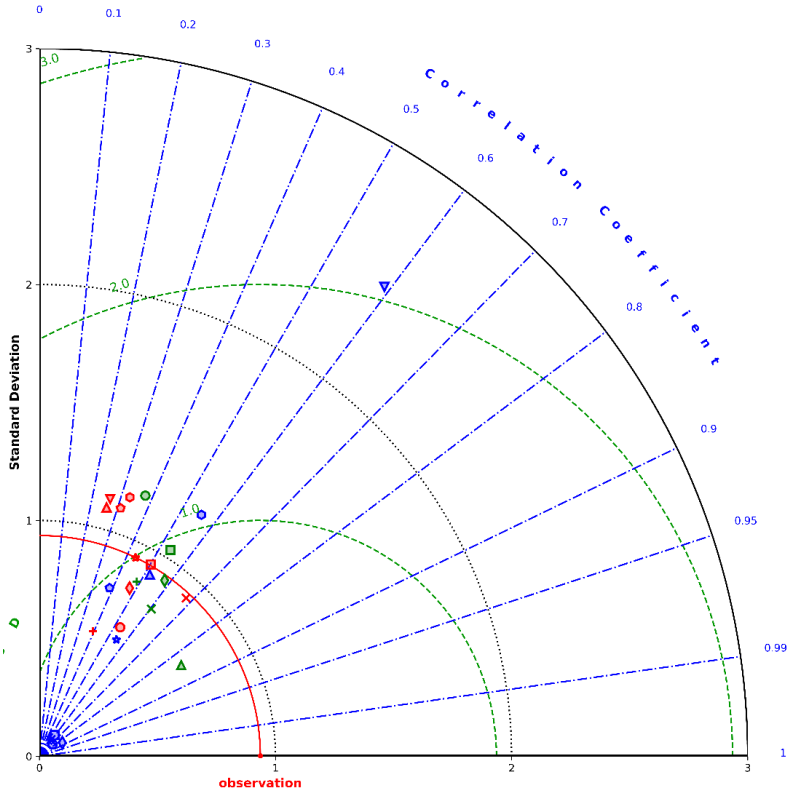

S1(m) Taylor diagram for station GMB3001

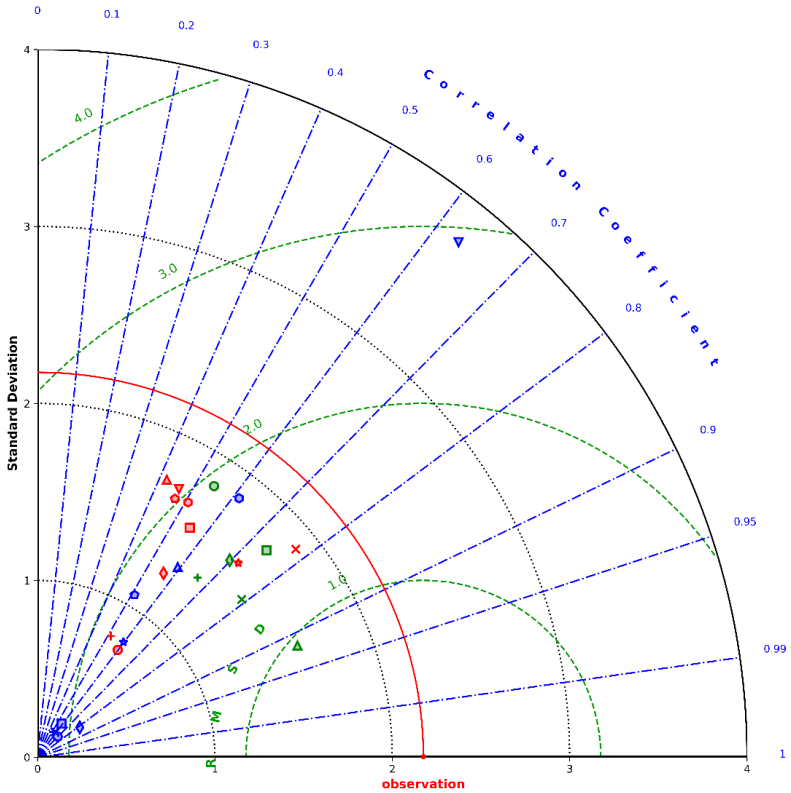

S1(n) Taylor diagram for station LBR3001

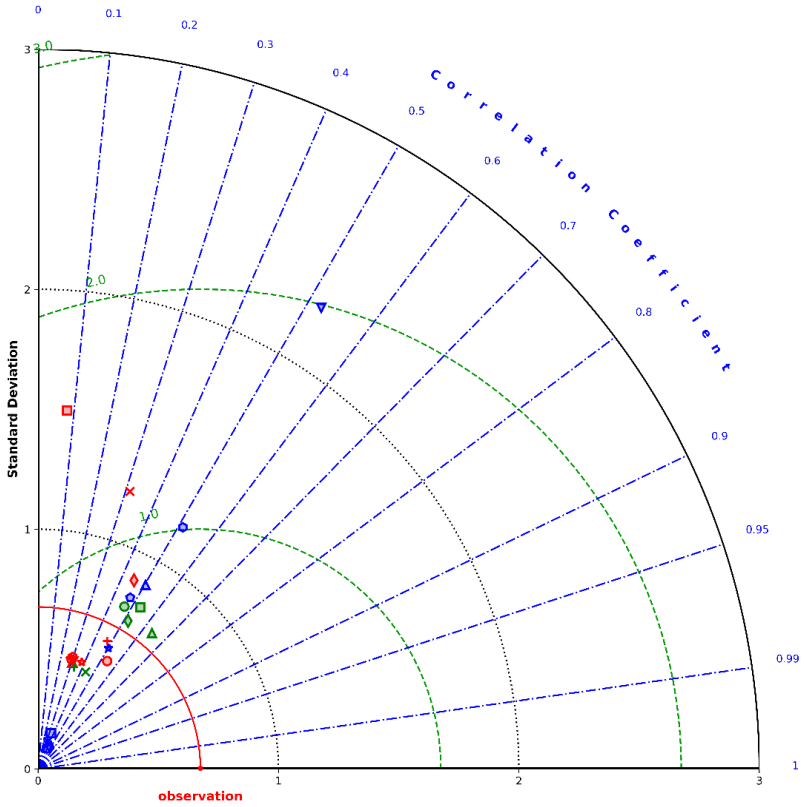

S1(o) Taylor diagram for station NER3001

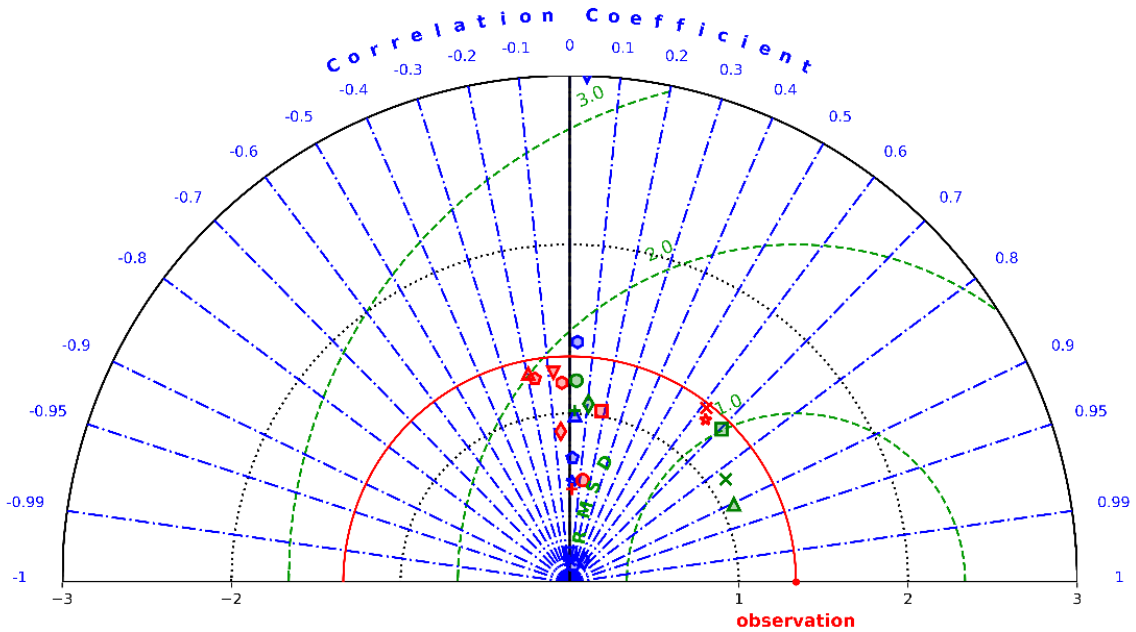

S1(p) Taylor diagram for station NGA3001

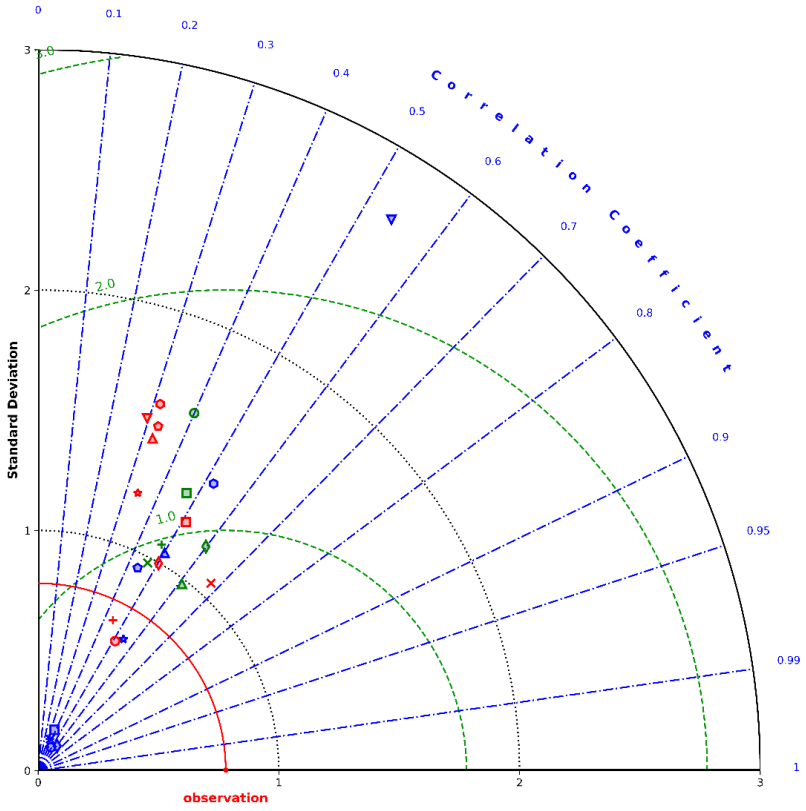

S1(q) Taylor diagram for station SEN3001

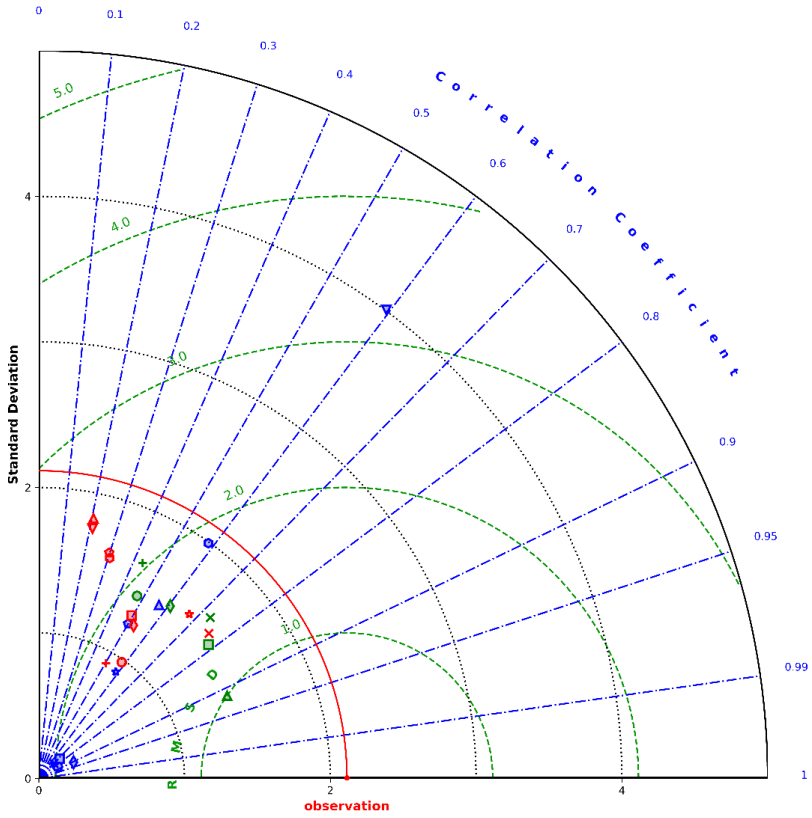

S1(r) Taylor diagram for station SEN4001

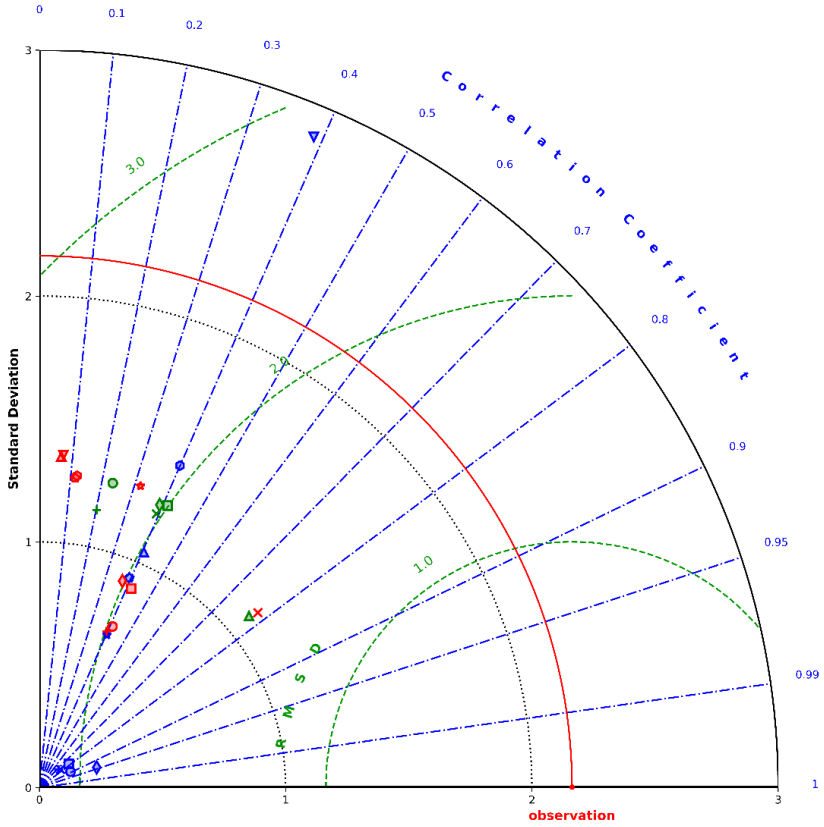

S1(s) Taylor diagram for station SLE3002

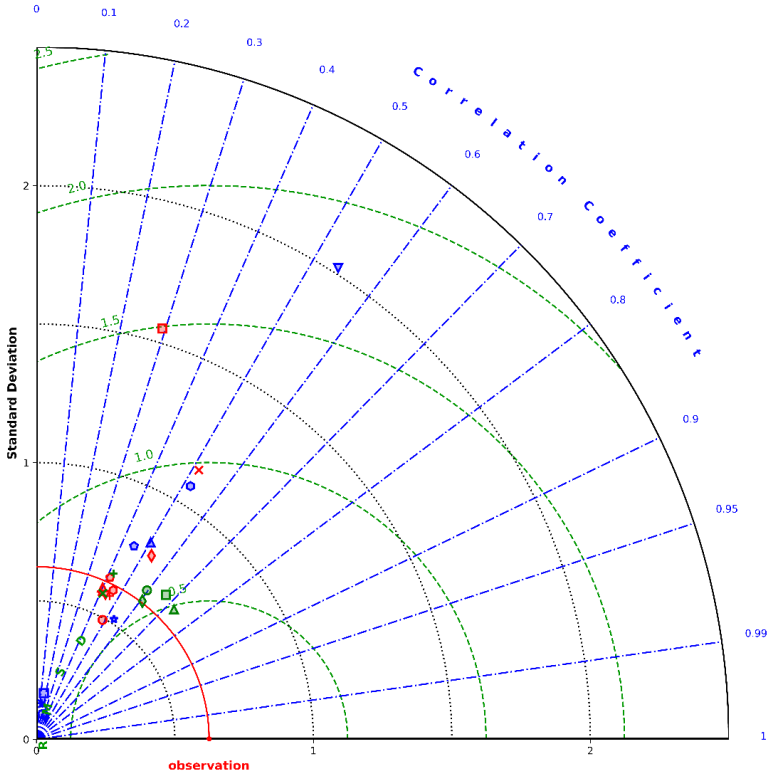

S1(t) Taylor diagram for station TCD3001

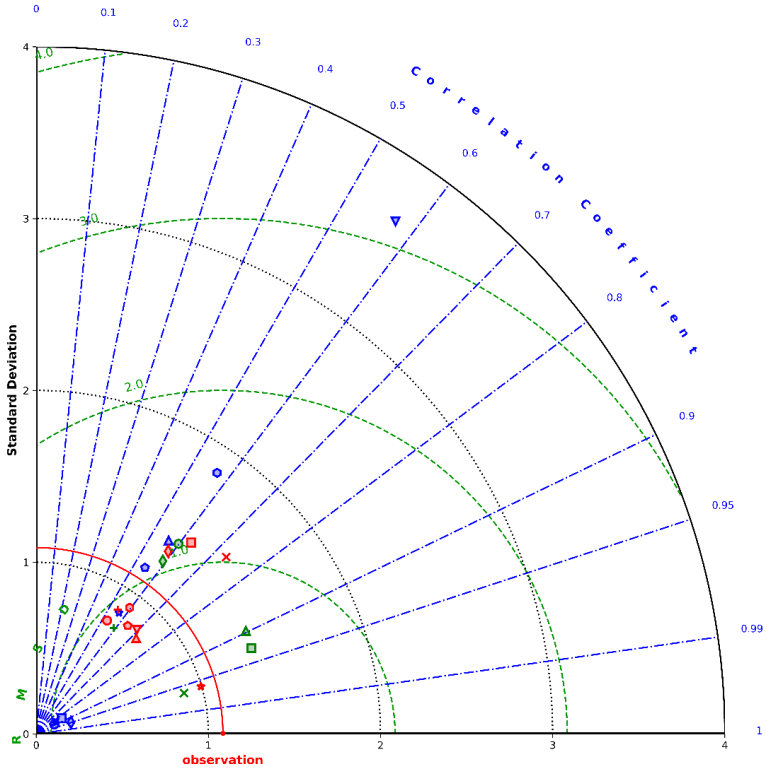

S1(u) Taylor diagram for station TGO3001

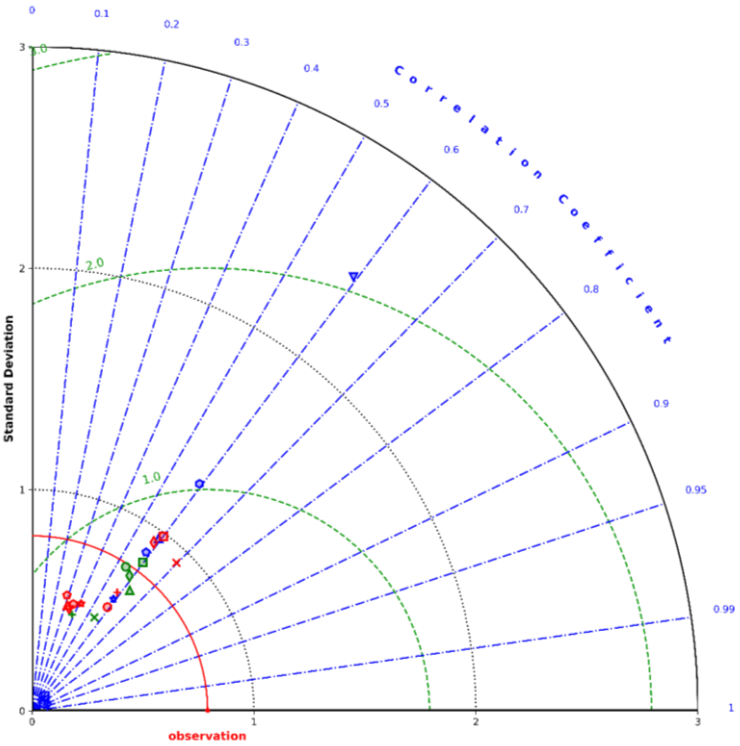

S1(v) Symbol legend for plotted models

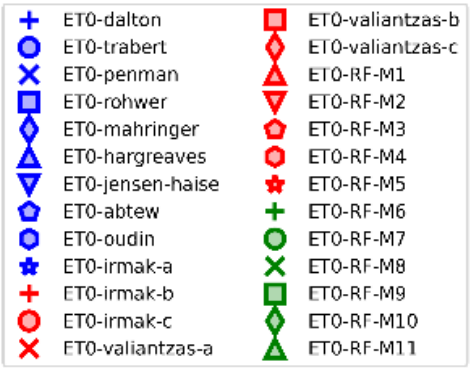

Supplementary Tables

Supplementary Table 1

Summary of Selected Literature on Machine Learning Applications for ET0 Estimation

This table presents a curated selection of recent studies that compare and utilise machine learning methods to estimate reference evapotranspiration (ET0). The literature compilation was achieved through a search for "machine learning ET0 estimation" in Google Scholar for the years 2016-2021. The table collates the most pertinent studies identified in the initial pages of search results, with additional relevant papers supplemented by the authors' further reading.

Reference	**Compared machine learning models**	**Origin and type of data**	**Climate**	**Location**
(Feng et al., 2016)	extreme learning machine (ELM), neural networks optimized by genetic algorithm (GANN), wavelet neural networks (WNN)	13 weather stations, 1994-2013 period, daily data	warm humid	Central Sichuan, China
(Gocic et al., 2016)	ELM	2 weather stations, 1980-2010 period, daily data	ND	Serbia
(Kisi, 2016)	least square support vector regression (LSSVR), multivariate adaptive regression splines (MARS), M5Tree	2 weather stations, 1982-2006 period, monthly data	mediterranean	Western Turkey
(Patil and Deka, 2016)	ELM, artificial neural networks (ANN), least square support vector machine (LSSVM)	2 weather stations, 1970-2010 period, weekly data	arid	Rajastan, India

(Yassin et al., 2016)	ANN, gene expression programming (GEP)	19 weather stations, 1980-2010 period, daily data	arid	Saudi Arabia
(Yin et al., 2017)	Genetic algorithm support vector machine (GA-SVM), ANN	1 weather station, 2009-2010 period, daily data	temperate	Qilian Mountains, NW China
(Antonopoulos and Antonopoulos, 2017)	ANN	1 weather station, 2009-2013 period, daily data	mediterranean	Greece
(Feng et al., 2017a)	random forest (RF), generalized regression neural network (GRNN)	2 weather stations, 2009-2014 period, daily data	warm humid	Sichuan, SW China
(Feng et al., 2017b)	ELM, GRNN	6 weather stations, 1961-2014 period, daily data	warm humid	Sichuan, SW China
(Karimi et al., 2017)	GEP, support vector machine (SVM)	8 weather stations, 1997-2006 period, daily data	humid	South Korea
(Mehdizadeh et al., 2017)	GEP, polynomial SVM, radial basis function SVM, MARS	44 weather stations, 1951-2010 period, monthly data	arid	Iran
(Pandey et al., 2017)	evolutionary regression (ER), ANN, multi-nonlinear regression (MNLR), SVM	2 weather stations, 2008-2012 period, daily data	ND	Arunacha Pradesh, India
(Fan et al., 2018)	RF, M5Tree, gradient boosting decision tree (GBDT), extreme gradient boosting/XGBoost	8 weather stations, 1961-2010 period, daily data	various	China

	(XGB), SVM, ELM			
(Keshtegar et al., 2018)	adaptive neuro-fuzzy inference system (ANFIS), M5Tree, ANN	3 weather stations, 20 year data (period unknown), daily data	cold arid	Central Anatolia, Turkey
(Kisi and Alizamir, 2018)	wavelet extreme learning machine (WELM), WNN, ANN, online sequential ELM (OS-ELM)	2 weather stations, 1985-2005 period, daily data	semi arid	Central Anatolia, Iran
(Mehdizadeh, 2018)	MARS, GEP with lagged ET0	6 weather stations, 2000-2014 period, daily data	semi arid, arid, hyper arid	Iran
(Zhang et al., 2018)	SVM, ANN, ANFIS	9 weather stations, MODIS remote sensing data, 2010-2013 period, daily data	ND	Hexi corridor, NW China
(Ehteram et al., 2019)	SVM with cuckoo algorithm (SVM-CA), gaussian process regression (GPR), M5Tree, ANFIS	1 weather station, 1990-2016 period, daily data	humid	Himalaya, India
(Ferreira et al., 2019)	ANN, SVM	203 weather stations, 2001-2015 period, daily data	various	Brazil
(Granata, 2019)	M5Tree, bagging, RF, support vector regression (SVR)	1 weather station, 2000-2004 period, daily data	subtropical humid	Florida, USA
(Huang et al., 2019)	gradient boosting with categorical features support/CatBoost (CAT),	5 weather stations, 2001-2015 period,	humid	southern China

	RF, SVM	daily data		
(Mosavi and Edalatifar, 2019)	ANFIS, particle swarm optimization (PSO), principal component analysis (PCA)	2 weather stations, 1981-2011 period, monthly data	arid	Iran
(Nourani et al., 2019)	feed forward ANN, ANFIS, SVR	14 weather stations, 1987-2018 period, monthly data	various	Turkey, Cyprus, Iran, Iraq, Lybia
(Reis et al., 2019)	ANN, ELM, multiple linear regression (MLR)	5 weather stations, 1996-2016 period, daily data	warm tropical, dry winter	Verde Grande Basin, Brazil
(Wu and Fan 2019)	multi-layer perceptron (MLP), GRNN, ANFIS, SVM, kernel-based nonlinear extension of Arps decline (KNEA), M5Tree, XGB, MARS	14 weather stations, 2001-2015 period, daily data	various	China
(Wu et al., 2019)	ANN, RF, GBDT, XGB, MARS, SVM, ELM, KNEA	11 weather stations, 2011-2015 period, daily data	subtropical humid	Jiangxi province, China
(Zhang et al. 2019)	SVM	5 weather stations, 1990-2014 period, daily data	ND	Shaangxi, China
(Ashrafzadeh et al., 2020)	seasonal autoregressive integrated moving average (SARIMA), SVM	4 weather stations, 1993-2014 period, daily data	ND	Northern Iran
(Chia et al., 2020)	SVM	4 weather stations 2014-2018 period, daily data	tropical	west coast Malaysia
(Dos Santos	cubist regression, ANN, SVM,	23 weather stations,	various	MATOPIBA,

Farias et al., 2020)	MLR	2000-2016 period, daily data		Brasil
(Hossein Kazemi et al., 2020)	GEP	7 weather stations, 2008-2017 period, daily data	arid	Iran
(Kim et al., 2020)	RF	9 weather stations + MODIS remote sensing data + numerical weather prediction data, 2013-2019 period, daily data	ND	South Korea
(Mohammadi and Mehdizadeh, 2020)	SVR with whale optimization algorithm (WOA)	3 weather stations, 2000-2014 period, daily data	semi arid, arid, hyper arid	Iran
(Wu et al., 2020)	Adaptive boosting (ADA), GBDT, XGB, light gradient boosting decision machine (LGB), CAT	10 weather stations, 1997-2016 period, daily data	temperate, subtropical and tropical	eastern monsoon zone, China
(Yu et al., 2020)	ANN, SVR, ELM	1 weather station, 2005-2017 period, daily data	semiarid, arid	Xinjiang Uygur, China
(Zhang et al., 2020)	CAT, GRNN, RF	15 weather stations, 1996-2015 period, daily data	arid, semi-arid	northern China
(Adnan et al., 2020)	ANN, MARS, M5Tree	2 weather stations, 1968-2015 period, daily data	mediterranean	southern Turkey

(Ayaz et al., 2021)	LSTM, GBDT, RF, SVR	2 weather stations, 1965-2015 period, daily data	hot semi arid, west coast marine climate	Hyderabad, India, Waipara, New Zealand
(Bellido-Jiménez et al., 2021)	MLP, ELM, GRNN, SVM, RF, XGB	5 weather stations, 2000-2018 period, daily data	semi arid	Andalusia, Spain
(Chia et al., 2021a)	MLP, SVM, ANFIS, bootstrap aggregating, Bayesian model averaging (BMA), ELM	4 weather stations, undetermined period, daily data	ND	peninsular Malaysia
(Chia et al., 2021b)	ELM-PSO hybrid, ELM-moth-flame optimization (MFO) hybrid, ELM-WOA hybrid	3 weather stations, 2014-2018 period, daily data	tropical	Eastern Malaysia
(Rashid Niaghi et al., 2021)	GEP, SVM, MLR, RF	6 weather stations, 2003-2016 period, daily data	continental	North Dakota and Minnesota, USA
(Sattari et al., 2021)	GPR, SVR, Broyden Fletcher Goldfarb Shanno ANN, LSTM	1993-2018 period, monthly regional measurements	arid, semi-arid	Turkey
(Wu et al., 2021)	ELM coupled with K-means clustering and firefly algorithms, ANFIS, RF, M5Tree	26 weather stations, 1966-2015 period, monthly data	ND	Poyang Lake basin, Southern China
(Yan et al., 2021)	XGB-WOA	8 weather stations, 1966-2015 period, daily data	arid, humid	China

References for supplementary materials

Adnan, R.M., Heddam, S., Yaseen, Z.M., Shahid, S., Kisi, O., Li, B., 2020. Prediction of Potential Evapotranspiration Using Temperature-Based Heuristic Approaches. Sustainability 13, 297. https://doi.org/10.3390/su13010297

Antonopoulos, V.Z., Antonopoulos, A.V., 2017. Daily reference evapotranspiration estimates by artificial neural networks technique and empirical equations using limited input climate variables. Comput. Electron. Agric. 132, 86–96. https://doi.org/10.1016/j.compag.2016.11.011

Ashrafzadeh, A., Kişi, O., Aghelpour, P., Biazar, S.M., Masouleh, M.A., 2020. Comparative Study of Time Series Models, Support Vector Machines, and GMDH in Forecasting Long-Term Evapotranspiration Rates in Northern Iran. J. Irrig. Drain. Eng. 146, 04020010. https://doi.org/10.1061/(ASCE)IR.1943-4774.0001471

Ayaz, A., Rajesh, M., Singh, S.K., Rehana, S., Lab for Spatial Informatics, International Institute of Information Technology, Hyderabad, India, National Institute of Water & Atmospheric Research Ltd (NIWA), New Zealand, 2021. Estimation of reference evapotranspiration using machine learning models with limited data. AIMS Geosci. 7, 268–290. https://doi.org/10.3934/geosci.2021016

Bellido-Jiménez, J.A., Estévez, J., García-Marín, A.P., 2021. New machine learning approaches to improve reference evapotranspiration estimates using intra-daily temperature-based variables in a semi-arid region of Spain. Agric. Water Manag. 245, 106558. https://doi.org/10.1016/j.agwat.2020.106558

Chia, M.Y., Huang, Y.F., Koo, C.H., 2021a. Swarm-based optimization as stochastic training strategy for estimation of reference evapotranspiration using extreme learning machine. Agric. Water Manag. 243, 106447. https://doi.org/10.1016/j.agwat.2020.106447

Chia, M.Y., Huang, Y.F., Koo, C.H., 2021b. Improving reference evapotranspiration estimation using novel inter-model ensemble approaches. Comput. Electron. Agric. 187, 106227. https://doi.org/10.1016/j.compag.2021.106227

Chia, M.Y., Huang, Y.F., Koo, C.H., 2020. Support vector machine enhanced empirical reference evapotranspiration estimation with limited meteorological parameters. Comput. Electron. Agric. 175, 105577. https://doi.org/10.1016/j.compag.2020.105577

Dos Santos Farias, D.B., Althoff, D., Rodrigues, L.N., Filgueiras, R., 2020. Performance evaluation of numerical and machine learning methods in estimating reference evapotranspiration in a Brazilian agricultural frontier. Theor. Appl. Climatol. 142, 1481–1492. https://doi.org/10.1007/s00704-020-03380-4

Ehteram, M., Singh, V.P., Ferdowsi, A., Mousavi, S.F., Farzin, S., Karami, H., Mohd, N.S., Afan, H.A., Lai, S.H., Kisi, O., Malek, M.A., Ahmed, A.N., El-Shafie, A., 2019. An improved model based on the support vector machine and cuckoo algorithm for simulating reference evapotranspiration. PLOS ONE 14, e0217499. https://doi.org/10.1371/journal.pone.0217499

Fan, J., Yue, W., Wu, L., Zhang, F., Cai, H., Wang, X., Lu, X., Xiang, Y., 2018. Evaluation of SVM, ELM and four tree-based ensemble models for predicting daily reference evapotranspiration using limited meteorological data in different climates of China. Agric. For. Meteorol. 263, 225–241. https://doi.org/10.1016/j.agrformet.2018.08.019

Feng, Y., Cui, N., Gong, D., Zhang, Q., Zhao, L., 2017a. Evaluation of random forests and generalized regression neural networks for daily reference evapotranspiration modelling. Agric. Water Manag. 193, 163–173. https://doi.org/10.1016/j.agwat.2017.08.003

Feng, Y., Cui, N., Zhao, L., Hu, X., Gong, D., 2016. Comparison of ELM, GANN, WNN and empirical models for estimating reference evapotranspiration in humid region of Southwest China. J. Hydrol. 536, 376–383. https://doi.org/10.1016/j.jhydrol.2016.02.053

Feng, Y., Peng, Y., Cui, N., Gong, D., Zhang, K., 2017b. Modeling reference evapotranspiration using extreme learning machine and generalized regression neural network only with temperature data. Comput. Electron. Agric. 136, 71–78. https://doi.org/10.1016/j.compag.2017.01.027

Ferreira, L.B., Da Cunha, F.F., De Oliveira, R.A., Fernandes Filho, E.I., 2019. Estimation of reference evapotranspiration in Brazil with limited meteorological data using ANN and SVM – A new approach. J. Hydrol. 572, 556–570. https://doi.org/10.1016/j.jhydrol.2019.03.028

Gocic, M., Petković, D., Shamshirband, S., Kamsin, A., 2016. Comparative analysis of reference evapotranspiration equations modelling by extreme learning machine. Comput. Electron. Agric. 127, 56–63. https://doi.org/10.1016/j.compag.2016.05.017

Granata, F., 2019. Evapotranspiration evaluation models based on machine learning algorithms—A comparative study. Agric. Water Manag. 217, 303–315. https://doi.org/10.1016/j.agwat.2019.03.015

Hossein Kazemi, M., Shiri, J., Marti, P., Majnooni-Heris, A., 2020. Assessing temporal data partitioning scenarios for estimating reference evapotranspiration with machine learning techniques in arid regions. J. Hydrol. 590, 125252. https://doi.org/10.1016/j.jhydrol.2020.125252

Huang, G., Wu, L., Ma, X., Zhang, W., Fan, J., Yu, X., Zeng, W., Zhou, H., 2019. Evaluation of CatBoost method for prediction of reference evapotranspiration in humid regions. J. Hydrol. 574, 1029–1041. https://doi.org/10.1016/j.jhydrol.2019.04.085

Karimi, S., Kisi, O., Kim, S., Nazemi, A.H., Shiri, J., 2017. Modelling daily reference evapotranspiration in humid locations of South Korea using local and cross-station data management scenarios. Int. J. Climatol. 37, 3238–3246. https://doi.org/10.1002/joc.4911

Keshtegar, B., Kisi, O., Ghohani Arab, H., Zounemat-Kermani, M., 2018. Subset Modeling Basis ANFIS for Prediction of the Reference Evapotranspiration. Water Resour. Manag. 32, 1101–1116. https://doi.org/10.1007/s11269-017-1857-5

Kim, N., Kim, K., Lee, S., Cho, J., Lee, Y., 2020. Retrieval of Daily Reference Evapotranspiration for Croplands in South Korea Using Machine Learning with Satellite Images and Numerical Weather Prediction Data. Remote Sens. 12, 3642. https://doi.org/10.3390/rs12213642

Kisi, O., 2016. Modeling reference evapotranspiration using three different heuristic regression approaches. Agric. Water Manag. 169, 162–172. https://doi.org/10.1016/j.agwat.2016.02.026

Kisi, O., Alizamir, M., 2018. Modelling reference evapotranspiration using a new wavelet conjunction heuristic method: Wavelet extreme learning machine vs wavelet neural networks. Agric. For. Meteorol. 263, 41–48. https://doi.org/10.1016/j.agrformet.2018.08.007

Mehdizadeh, S., 2018. Estimation of daily reference evapotranspiration (ETo) using artificial intelligence methods: Offering a new approach for lagged ETo data-based modeling. J. Hydrol. 559, 794–812. https://doi.org/10.1016/j.jhydrol.2018.02.060

Mehdizadeh, S., Behmanesh, J., Khalili, K., 2017. Using MARS, SVM, GEP and empirical equations for estimation of monthly mean reference evapotranspiration. Comput. Electron. Agric. 139, 103–114. https://doi.org/10.1016/j.compag.2017.05.002

Mohammadi, B., Mehdizadeh, S., 2020. Modeling daily reference evapotranspiration via a novel approach based on support vector regression coupled with whale optimization algorithm. Agric. Water Manag. 237, 106145. https://doi.org/10.1016/j.agwat.2020.106145

Mosavi, A., Edalatifar, M., 2019. A Hybrid Neuro-Fuzzy Algorithm for Prediction of Reference Evapotranspiration, in: Laukaitis, G. (Ed.), Recent Advances in Technology Research and Education, Lecture Notes in Networks and Systems. Springer International Publishing, Cham, pp. 235–243. https://doi.org/10.1007/978-3-319-99834-3_31

Nourani, V., Elkiran, G., Abdullahi, J., 2019. Multi-station artificial intelligence based ensemble modeling of reference evapotranspiration using pan evaporation measurements. J. Hydrol. 577, 123958. https://doi.org/10.1016/j.jhydrol.2019.123958

Pandey, P.K., Nyori, T., Pandey, V., 2017. Estimation of reference evapotranspiration using data driven techniques under limited data conditions. Model. Earth Syst. Environ. 3, 1449–1461. https://doi.org/10.1007/s40808-017-0367-z

Patil, A.P., Deka, P.C., 2016. An extreme learning machine approach for modeling evapotranspiration using extrinsic inputs. Comput. Electron. Agric. 121, 385–392. https://doi.org/10.1016/j.compag.2016.01.016

Rashid Niaghi, A., Hassanijalilian, O., Shiri, J., 2021. Estimation of Reference Evapotranspiration Using Spatial and Temporal Machine Learning Approaches. Hydrology 8, 25. https://doi.org/10.3390/hydrology8010025

Reis, M.M., Da Silva, A.J., Zullo Junior, J., Tuffi Santos, L.D., Azevedo, A.M., Lopes, É.M.G., 2019. Empirical and learning machine approaches to estimating reference evapotranspiration based on temperature data. Comput. Electron. Agric. 165, 104937. https://doi.org/10.1016/j.compag.2019.104937

Sattari, M.T., Apaydin, H., Band, S.S., Mosavi, A., Prasad, R., 2021. Comparative analysis of kernel-based versus ANN and deep learning methods in monthly reference evapotranspiration estimation. Hydrol. Earth Syst. Sci. 25, 603–618. https://doi.org/10.5194/hess-25-603-2021

Wu, L., Peng, Y., Fan, J., Wang, Y., 2019. Machine learning models for the estimation of monthly mean daily reference evapotranspiration based on cross-station and synthetic data. Hydrol. Res. 50, 1730–1750. https://doi.org/10.2166/nh.2019.060

Wu, L., Peng, Y., Fan, J., Wang, Y., Huang, G., 2021. A novel kernel extreme learning machine model coupled with K-means clustering and firefly algorithm for estimating monthly reference evapotranspiration in parallel computation. Agric. Water Manag. 245, 106624. https://doi.org/10.1016/j.agwat.2020.106624

Wu, T., Zhang, W., Jiao, X., Guo, W., Hamoud, Y.A., 2020. Comparison of five Boosting-based models for estimating daily reference evapotranspiration with limited meteorological variables. PLOS ONE 15, e0235324. https://doi.org/10.1371/journal.pone.0235324

Yan, S., Wu, L., Fan, J., Zhang, F., Zou, Y., Wu, Y., 2021. A novel hybrid WOA-XGB model for estimating daily reference evapotranspiration using local and external meteorological data: Applications in arid and humid regions of China. Agric. Water Manag. 244, 106594. https://doi.org/10.1016/j.agwat.2020.106594

Yassin, M.A., Alazba, A.A., Mattar, M.A., 2016. Artificial neural networks versus gene expression programming for estimating reference evapotranspiration in arid climate. Agric. Water Manag. 163, 110–124. https://doi.org/10.1016/j.agwat.2015.09.009

Yin, Z., Wen, X., Feng, Q., He, Z., Zou, S., Yang, L., 2017. Integrating genetic algorithm and support vector machine for modeling daily reference evapotranspiration in a semi-arid mountain area. Hydrol. Res. 48, 1177–1191. https://doi.org/10.2166/nh.2016.205

Yu, H., Wen, X., Li, B., Yang, Z., Wu, M., Ma, Y., 2020. Uncertainty analysis of artificial intelligence modeling daily reference evapotranspiration in the northwest end of China. Comput. Electron. Agric. 176, 105653. https://doi.org/10.1016/j.compag.2020.105653

Zhang, Y., Zhao, Z., Zheng, J., 2020. CatBoost: A new approach for estimating daily reference crop evapotranspiration in arid and semi-arid regions of Northern China. J. Hydrol. 588, 125087. https://doi.org/10.1016/j.jhydrol.2020.125087

Zhang, Z., Gong, Y., Wang, Z., 2018. Accessible remote sensing data based reference evapotranspiration estimation modelling. Agric. Water Manag. 210, 59–69. https://doi.org/10.1016/j.agwat.2018.07.039